Study of a Neutron Star Low-Mass X-Ray Binary Observed in Outburst by NuSTAR and INTEGRAL in 2015

Frederik Lindskov Gaarde
June 2017

Supervisor: Jérôme Chenevez

DTU Space
National Space Institute

Abstract

This study investigates the thermonuclear bursting of the LMXB SAX J174853-202202, located in the globular cluster NGC 6440, observed by the Nuclear Spectroscopic Telescope Array (NuSTAR) and Joint European Monitor for X-rays (JEMX) on board the INTErnational Gamma-Ray Astrophysics Laboratory (INTEGRAL). 8 distinct burst was detected from the light curve, and a time resolved spectral analysis of the burst revealed one burst exhibiting photospheric radius expansion reaching Eddington luminosity limit $L_{\mathrm{Edd}} = 2.68 \times 10^{38}$ ergs s^{-1}. Combining light curves of NuSTAR and JEMX produced a more complete picture, but the data gaps of NuSTAR was not covered. The off-axis angle of JEMX was often high rendering the data ill-defined making data analysis complicated. SAX J174853-202202 became a ToO few days prior to the NuSTAR observation which provided well-defined data. JEMX-1 and 2 showed uncorrelated discrepancies in the flux readings making the data somewhat untrustworthy.

Contents

1 Introduction

A star of $8 - 20\,M_{\odot}$ will undergo core-collapse in its final stage of evolution. The collapse will leave a rapidly spinning, extremely dense neutron star (NS) of mass $1.4 - 3\,M_{\odot}$ and radius $10 - 20$ km. If the neutron star has a companion star of mass $< 1M_{\odot}$ it may accrete matter from this star. Such a system is known as a low-mass X-ray binary (LMXB). The accretion may trigger energetic X-ray bursts under the right circumstances which is detectable by astronomical telescopes in orbit around the Earth. The theory of the physics behind these outburst are described in Section 2.

The Nuclear Spectroscopic Telescope Array (NuSTAR) is a telescope by the National Aeronautics and Space Administration (NASA) that is capable detect the emissions from a burst of a LMXB. The telescope is in a near circular orbit around Earth. The telescope is comprised of detector and optic modules and a mast. NuSTAR and its data acquisition is described in Section 3.

The INTErnational Gamma-Ray Astrophysics Laboratory (INTEGRAL) is a satellite developed and launched by the European Space Agency (ESA), and is comprised of several telescopes. One of those is the Joint European Monitor for X-rays (JEMX), which is capable of detecting the X-rays emitted during outburst of LMXBs. The telescope consist of two co-aligned detectors. JEMX and its data acquisition is described in Section 4.

The source investigated in this study is the LMXB SAX J174853-202202, which lies in the globular cluster NGC 6440. It has been observed in outburst late February 2015 by both NuSTAR and JEMX. The two telescopes data will be used to produce light curves that can be used for spectral analysis. By using both NuSTAR and JEMX it is the hope that a complete light curve can be constructed so a detailed analysis can be performed. Data gaps will arise when the source is eclipsed by Earth, and as the bursts may last between $10 - 1000$ seconds its easy to miss a burst, which will have great impact on the results. The analysis of data is accounted for in Section 5.

A time resolved spectral analysis of the NuSTAR data will be conducted using the NASA developed tool `XSPEC`. This allows the characteristics of bursts to be plotted in several phases during the outburst. From the results it is possible to give estimates of parameters such as the accretion rate, the total energy released during a burst and material composition, to name a few. The results of the spectral analysis of the NuSTAR data is described in detail in Section 5.1.

The data from JEMX is analysed using ESAs own scripts and tools, and can be used to find the same parameters as mentioned above. A comparison of NuSTAR and JEMX can be made once the light curves of both instruments has been analysed. The data analysis of the JEMX data is described in detail in Section 5.2.

Finally a discussion of the results will be given in Section 6. Here possible explanations of the seen phenomena will be given, and choices made throughout the study will be accounted for. A conclusion in Section 7 will summarize the study of SAX J174853-202202, the work with NuSTAR and JEMX and results thereof.

2 Theory

In this section a more detailed description of the underlying physics of a NS will be given. First a short introduction how a massive star undergoes core-collapse supernova and becomes a NS. Following that, the method to categorise the X-ray source will be explained and the difference between the categories will be accounted for. Finally the physics behind the accretion process, the bursts of NS and the evolution of the NS will be accounted for.

2.1 The core-collapse supernova of a massive star

A star with sufficiently high mass, $8-20\,M_{\odot}$, will throughout its lifetime sustain thermonuclear fusion of hydrogen and helium at first while as the core compresses and gets hotter heavier elements may start to fuse. This cycle continues until neon starts to fuse into iron in the core. Iron requires a lot of energy to fuse into even heavier elements, thus iron is the final stage of thermonuclear fusion of the star, (Freedmann & Kaufmann, 2008).
Once the core contains enough iron it starts to contract very fast. This increases the temperature of the core to the magnitude of $5 \times 10^9\,\mathrm{K}$. At this temperature, gamma photons emitted carry so much energy that photodisintegration occurs, a process where gamma-ray photons are able to break the iron nuclei into helium nuclei. As the core gets even denser, electrons and protons are forced together to from neutrons and neutrinos, (Freedmann & Kaufmann, 2008):

$$\mathrm{e}^- + \mathrm{p} \rightarrow \mathrm{n} + \nu$$

The neutrinos will carry a lot of energy away forcing the core to compress even further until it reaches nuclear density. This produces a pressure wave that will be moving outwards from the core. The pressure wave receives energy from hot gas bubbles causing it to speed up until it reaches supersonics speeds, becoming a shock wave. As the shock wave thins out the outer layers of the star, the energy contained within is released creating a huge energy outburst. This phenomena is known as a core-collapse supernova.

Had the original star mass been below $8\,M_{\odot}$ the star would have evolved into a white dwarf. Had it been greater, around $20-25\,M_{\odot}$ or greater, the star would have evolved into a black hole. The ground between creates the neutron star, whose core, not surprisingly, is composed of primarily neutrons. The neutrons generate a degenerate neutron pressure that prevents the core from further collapse.

Since the momentum of the collapsing star has been conserved, the core spins very rapidly. From the poles of the NS beams of electromagnetic radiation is being emitted. If the beam can be detected on Earth, the spin period P of the NS can be determined (it would shine the Earth once for each spin period, like a light house). In order for NS, or any given object in fact, to not break apart, the centrifugal force felt by a mass m on the surface must be equal to the gravitational force:

$$\frac{mv^2}{R} = \frac{GMm}{R^2} \tag{1}$$

where $v = 2\pi R/P$. Thus the minimum radius of a NS can be estimated to be:

$$R < \left(\frac{GMP^2}{4\pi^2}\right)^{1/3} \tag{2}$$

The mass of neutron stars is usually in the range of $1-3\,M_{\odot}$, which supports neutrons stars to spin with frequencies up to about 1 kHz.

2.2 LMXB or HMXB

If the neutron star has a companion, it may accrete matter. If it does, the accreted matter can trigger X-ray bursts on the surface of the NS releasing vast amount of X-ray radiation detectable for instruments on Earth.

Two types of X-ray bursters exist: The low mass X-ray binary (LMXB) and the high mass X-ray binary (HMXB). The LMXB consist of a NS and a donor star of mass $< 1\,M_{\odot}$, often much less. The HMXB has a NS with a donor star massive enough to produce a stellar wind, typically an early-type massive $3 - 10\,M_{\odot}$ OB star, (Chenevez, b), (Seward & Charles, 2010).

Consider a binary system with a massive $8 - 20\,M_{\odot}$ star and a more ordinary Sun-like star. The massive star will cycle through its stages of evolution faster than the companion star, and will approximately $10^6 - 10^7$ years after birth undergo a core-collapse supernova leaving a neutron star behind. The compact object, the NS, and the companion star will continue to orbit each other, though likely with a different orbital period than before the supernova. At this point the NS is spinning very fast and will continue to do so while the companion star evolves, loosing only little rotation speed[1].

As the companion evolves and expands the Roche lobe will be filled and transfer of matter through inner Lagrangian point unto the surface of the NS, see Figure 1. The angular momentum of the matter is conserved and thus an accretion disc around the NS is formed. This is the characteristics for a LMXB. The accretion and ignition of the matter is described in detail in Section 2.3 and 2.4.

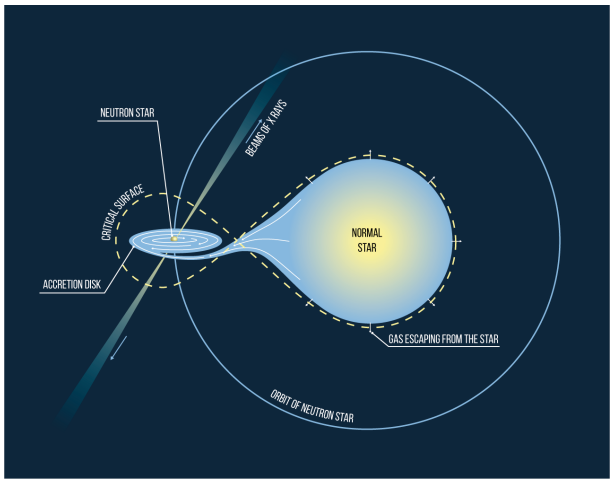

Figure 1: Donor star with its Roche Lobe filled allow matter to accrete unto the neutron star. Picture from MIPT (2016).

In the HMXB system, the NS accretes matter by being showered by matter from the stellar wind produced by its donor star, which is much larger than a star in LMXB system. When the layer of matter on the surface of the NS is thick enough, it will ignite and explode releasing huge amounts of X-ray radiation.

HMXB is usually located in the Galactic plane, while LMXB is typically older and is thus mostly distributed in the Galactic center, approximating the distance to about $5 - 10$ kpc. The activity of the HMXB depend on their orbit around the companion. If the orbit is highly elliptical there may long periods of inactivity.

The main focus of this study is the LMXB, and the theory necessary to complete the study of a burster is accounted for in section 2.3 and 2.4.

[1]The spin down rate denoted $\dot{P}$ is typically very low. For an example, the Crab pulsar have $\dot{P} = 10^{-12.4}$ s/s, Condon & Ransom (2016)

2.3 Accretion process

The matter accreted from the donor star is primarily hydrogen, helium or a mix of those, because of the nature of the donor. The matter in the accretion disc reaches high temperatures due to being irradiated by the NS and due to the friction between the matter itself. The acceleration of gravity on the surface of the NS can be determined, assuming the mass $M_{\mathrm{NS}} = 1.4\,M_{\odot}$ and radius $R = 12$ km:

$$F_{\mathrm{grav}} = m\,g_{\mathrm{NS}} = \frac{G\,M_{\mathrm{NS}}\,m}{R^2} \tag{3}$$

$$g_{\mathrm{NS}} = 1.3 \cdot 10^{12}\,\mathrm{m/s^2}$$

which is a staggering 10^{11} greater than that on Earth. The acceleration is so great that relativistic effects has to be taken into account. From an outside observer the NS would even appear larger since light behind the visible surface bends around becoming visible.

The rate of accretion, $\dot{m}$, is a measure of the amount of matter that falls unto a unit square centimetre on the NS per second. The total amount of matter that falls unto the entire surface of the NS per second is denoted $\dot{M}$. There is an upper limit to accretion rate which is called the Eddington accretion limit denoted $\dot{m}_{\mathrm{Edd}}$ and $\dot{M}_{\mathrm{Edd}}$. To understand this limit one must look at the luminosity of the compact object.

Luminosity, L, is measure of the amount of energy radiated by an object. The energy radiated will exert a pressure that in most cases are far less than the force of gravity. However, LMXBs will sometimes during a burst radiate so much energy that the pressure overcomes the gravitational force and start to 'blow' away any matter outside the NS. When this phenomena occurs, the luminosity is said to have reached the Eddington luminosity limit, denoted L_{Edd}.

The Eddington luminosity limit can be derived by balancing the gravitational force and the radiation force:

$$F_{\mathrm{grav}} = F_{\mathrm{rad}} \tag{4}$$

where F_{grav} is given in Equation (3). The radiation force can be expressed as[2]:

$$F_{\mathrm{rad}} = \frac{L\,\sigma_e\,m}{4\,\pi\,c\,m_p\,R^2}$$

From equation (4) the Eddington luminosity limit can be solved for:

$$L_{\mathrm{Edd}} = \frac{4\,\pi\,c\,G\,M\,m_p}{\sigma_c}$$

Which can be expressed in the more meaningful astronomical terms:

$$L_{\mathrm{Edd}} = 1.3 \times 10^{38}\,\frac{M}{M_{\odot}} \tag{5}$$

From L_{Edd} the Eddington accretion rate can be derived. The luminosity resulting from the accretion can be expressed as the rate of gravitational energy released on the surface of the NS[3]:

$$L = \frac{G\,M\,\dot{M}}{R}$$

The measure of the efficiency of converting matter into energy is expressed by $\eta = \frac{G\,M}{R\,c^2}$, and as such, the Eddington accretion rate can be expressed as:

$$\dot{M}_{\mathrm{Edd}} = \frac{L_{\mathrm{Edd}}}{\eta\,c^2} \tag{6}$$

which per unit area is:

$$\dot{m}_{\mathrm{Edd}} = \frac{\dot{M}_{\mathrm{Edd}}}{4\,\pi\,R^2} \tag{7}$$

[2]Source: (Cotter, 2012)
[3]Source: (Seward & Charles, 2010)

For neutron stars the efficiency is approximately $\eta \sim 0.2$, (Chenevez, a), while it for black holes is $0.06 - 0.42$, 0.001 for white dwarfs and $0.01 - 0.001$ for nuclear reactions, Seward & Charles (2010). Neutron stars is thus most efficient at converting matter into energy.

During the accretion process a phenomena known as comptonization likely occurs. A cloud of hot plasma surrounds the accretion disc and the NS. When photons in the cloud is struck by an ultra-relativistic electrons emitted from the NS, they transfer the energy to the photons. These photons may be detected by X-ray telescopes as high energy tails of the burst.

The emissions from the accretion disc is known as the persistent.

2.4 Ignition of accumulated layer

Once a layer matter has formed on the surface of the NS, the density and temperature on the bottom gets so high, that the matter/fuel begins a thermonuclear burning process. Depending on whether H or He, or a mix of those, is present, different processes takes place. The rate of accretion also plays an important role on the burst composition.

According to (Galloway et al., 2008) different regimes of thermonuclear ignition exist depending on accretion rate expressed as a fraction of the local Eddington accretion rate.

At ($\lesssim 0.01\,\dot{m}_{\mathrm{Edd}}$), hydrogen burns thermally unstable which triggers a mixed helium and hydrogen burning. The resulting burst is a type I X-ray burst. Type I burst are long, lasting more than $100 - 1000$ seconds, because of the rapid proton process. The rp process is a series of proton captures and β decays, where the proton capure is very fast, but the β decay is rather slow, which effectively slows the burst down. The tail of these bursts are thus the effect of the rp process.

At ($\lesssim 0.01\,\dot{m}_{\mathrm{Edd}} \lesssim 0.1$), hydrogen burns stable in the hot CNO cycle into helium, see figure 2. As the helium layer grows at the base of the accreted matter, it steadily heats up until helium ignition occurs. Helium burns via the triple-α process which has no β decay limiting the speed of the burning and thus burns very unstably and fast. This is known as a helium flash. These very violent burst frequently cause a phenomena called photospheric radius expansion (PRE). More on PRE further down this section.

At ($\lesssim 0.1\,\dot{m}_{\mathrm{Edd}} \lesssim 1.0$), hydrogen is accreted faster than it is consumed, so when the helium ignites, it does so in a hydrogen rich environment. This causes the bursts to last > 10 seconds due to rp-process.

If $\dot{m}$ is greater than the $\dot{m}_{\mathrm{Edd}}$, stable helium burning depletes the fuel reserves, causing the burst activities to cease all together. If the donor star is a white dwarf, the accreted matter will be pure helium, which triggers intermediate long bursts. If a carbon layer at the base of the accreted matter has formed and is ignited, it will cause a superburst that last for hours.

While the accretion rate gives a good idea which kind of burst to expect, several other factors may play an important role. Certain reactions may remove a catalysts from the CNO-cycle, (Galloway et al., 2008). This can cause hydrogen and helium to burn steadily and stable, such that bursts activity may cease at an accretion rate of only $\dot{m}_{\mathrm{Edd}} \gtrsim 0.3$. Observation does show however, that this cannot explain all non-bursting sources at $\dot{m}_{\mathrm{Edd}} \gtrsim 0.3$.

The element composition at the base of the layer can vary over time, such that helium for an example could build up causing very energetic bursts for even low accretion rates ($\lesssim 0.01\,\dot{m}_{\mathrm{Edd}}$).

Also, the accreted matter may not be distributed evenly over the surface of the NS. A bulge forms around the NS in the plane of the accretion disc, see figure 3. The ignition is thus expected to start somewhere in the bulge and spread from there. The spread of the thermonuclear explosion may be affected by the rapid spin of the NS resulting in a anisotropic explosion. For spin periods of $0.01 - 0.001$ seconds assuming $R = 12$ km, an observer on the surface of the NS would be moving between 2.5% and 25% of the speed of light, which is enough for relativistic effects to affect the spread.

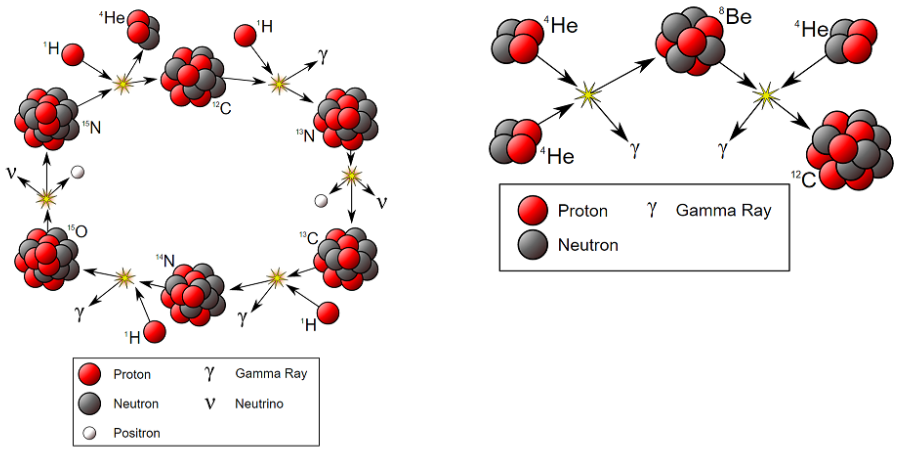

Figure 2: The hot CNO-cycle (left) and the triple-α process (left). Picture from: `https://commons.wikimedia.org/w/index.php?curid=691758` and `https://commons.wikimedia.org/w/index.php?curid=697609`.

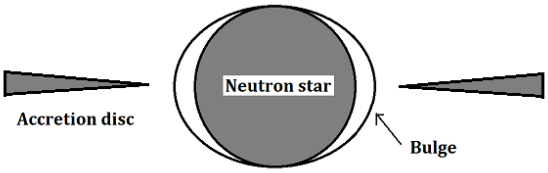

Figure 3: Illustration of the bulge created on the surface of the neutron star.

A measure of the composition of a burst is the α parameter which is ratio of the energy energy of the persistent and the burst. The involves finding the fluence is flux of a burs, denoted E_{b}, and the fluence of the persistent, E_{pers}. The fluence is found by a time resolved spectral analysis. This outputs a bolometric flux. By integrating the fluxes from each stage of the burst over time the fluence is retrieved. The fluence of the persistent prior to the burst is found be measuring the average persistent flux and multiplying this with the time between the burst and the previous burst. α can now be computed by the following formula, (Chenevez, b):

$$\alpha = \frac{F_{\mathrm{pers}}}{E_{\mathrm{b}}} t_{\mathrm{rec}} \tag{8}$$

E_{b} may also be found by using the fact that the decay of a burst appears to follow an exponential decay with decay time τ, peak flux F_{peak} and burst duration δt:

$$E_{\mathrm{b}} = F_{\mathrm{peak}}\, \tau \left(1 - e^{-\Delta t/\tau}\right) \tag{9}$$

α can also be found by a ratio of the gravitational energy released from matter falling unto the NS and the energy release of nuclear burning:

$$\alpha = \frac{E_{\mathrm{grav}}}{E_{\mathrm{nuc}}}$$

The value of α gives an estimate of the composition of the burst:

- $\alpha \approx 150$ signals mixed H/He burning triggered by hydrogen ignition, ($\lesssim 0.01\, \dot{m}_{\mathrm{Edd}}$).
- $\alpha \approx 200$ signals a helium flash and the burst often exhibit PRE, ($\lesssim 0.01\, \dot{m}_{\mathrm{Edd}} \lesssim 0.1$).
- $\alpha \approx 20 - 100$ signals mixed H/He burning triggered by unstable helium ignition, ($\lesssim 0.1\, \dot{m}_{\mathrm{Edd}} \lesssim 1.0$)

Photospheric radius expansions are interesting, as the luminosity required to triggers this phenomena is exactly the local L_{Edd}, which is relatively easy to determine. From L_{Edd} the distance to the source can be determined using the fact that a LMXB resembles a black body, and thus Stefan-Boltzmanns law hold:

$$L = 4\,\pi\,d^2\,F \leq L_{\text{Edd}} \tag{10}$$

which infers an upper limit to the distance, (Chenevez, b):

$$d \leq \sqrt{\frac{L_{\text{Edd}}}{4\,\pi\,F}} \tag{11}$$

Due to the strong gravitationally pull of the NS, matter is going experience a redshift denoted $(1+z)$ as it falls unto the surface of the NS. Factoring this into Equation (7) yields:

$$\dot{m} = \frac{\dot{M}}{4\,\pi\,R^2}(1+z) \tag{12}$$

The total accretion rate $\dot{M}$ can be found using the luminosity of the accretion disc between two bursts, denoted L_{pers}, and the burning efficient η:

$$\dot{M} = \frac{L_{\text{pers}}}{\eta\,c^2} \tag{13}$$

L_{pers} can be found by measuring the flux between two bursts. In this interval, the only flux measured should come from the accretion disc, denoted F_{pers}. The relationship between luminosity and flux is:

$$L_{\text{pers}} = 4\,\pi\,d^2\,\xi_{\text{p}} F_{\text{pers}} \tag{14}$$

where ξ_{p} is the isotropy factor describing the isotropy of the persistent. Assuming isotropy, $\dot{m}$ can now be written as:

$$\dot{m} = \left(\frac{d}{R_{\text{NS}}}\right)^2 \frac{F_{\text{pers}}}{\eta\,c^2}\,(1+z) \tag{15}$$

Knowing the accretion rate and the time between two burst, the ignition column depth can be determined:

$$y = \dot{m}\,\Delta t\,(1+z)^{-1} \tag{16}$$

The unit of y is [g/cm^2]. Thus, the total mass burned during a burst is:

$$M_{\text{b}} = 4\,\pi\,R_{\text{NS}}^2\,y \tag{17}$$

The recurrence time between bursts can be estimated as:

$$\Delta t = \frac{\xi_{\text{b}}}{\xi_{\text{p}}}\frac{E_{\text{b}}}{F_{\text{Pers}}}\,\frac{\eta\,c^2}{\varepsilon}\,(1+z) \tag{18}$$

where $\xi_{\text{b}}/\xi_{\text{p}}$ is the ratio of isotropy of the burst and persistent and ε is the energy efficiency. Combining Equation (18) and (8) yields the energy efficiency:

$$\varepsilon = \frac{\xi_{\text{b}}}{\xi_{\text{p}}}\,\frac{\eta\,c^2}{\alpha}\,(1+z) \tag{19}$$

From this, the total energy released by a burst can be found as:

$$E_{\text{b,rel}} = \frac{M_{\text{b}}}{1+z}\,\varepsilon \tag{20}$$

The energy release is typically in the order of $E_{\text{b,rel}} \approx 10^{40}$ ergs.

The material composition can now to be estimated. When ε is found, the energy per nucleon helps find out how much hydrogen the burst consisted of:

$$\varepsilon = Q_{\text{nuc}} \cdot 10^{18}\,\text{erg g}^{-1} \approx 1.6 + 4\,X \tag{21}$$

Solving for X yields the hydrogen to other matter ratio. But since the NS accretes matter from the donor stars shell, its a ratio of hydrogen to helium. When $X = 1$ its pure hydrogen, while $X = 0$ is no hydrogen.

3 NuSTAR

This section covers the astronomical telescope NuSTAR launched by NASA in 2012. NuSTARoperates in the energy band $3-78$ keV. It has a small field of view (FOV), but in turn have high spatial and spectral resolution. NuSTARwas launched from the Reagan Test Site on the Kwajalein Atoll in the South Pacific in order to deploy into a low-inclination orbit where passages through the South Atlantic Anomaly (SAA) are minimized. The orbit is 650×610 km, and takes approximately 90 minutes to complete an orbit, (Harrison et al., 2013)

The mission was launched to pursue five primary scientific objectives (from (Harrison et al., 2013)):

1. Probe obscured active galactic nucleus (AGN) activity out to the peak epoch of galaxy assembly in the universe (at $z \lesssim 2$) by surveying selected regions of the sky.
2. Study the population of hard X-ray-emitting compact objects in the Galaxy by mapping the central regions of the Milky Way.
3. Study the non-thermal radiation in young supernova remnants, both the hard X-ray continuum and the emission from the radioactive element ^{44}Ti.
4. Observe blazars contemporaneously with ground-based radio, optical, and TeV telescopes, as well as with Fermi and Swift, to constrain the structure of AGN jets.
5. Observe line and continuum emission from core-collapse supernovae in the Local Group, and from nearby Type Ia events, to constrain explosion models.

Objective 2) and 5) are essential as these provide the data necessary to conduct the study of a X-ray bursting NS. NuSTARconsist of two co-aligned hard X-ray telescope, which each has an optics module and a detector module. The optics modules uses Wolter-I conical approximation X-ray optics which focuses photons into detectors 10.14 meters away. The detectors and optics are held together by a composite mast that deploys after the instrument is in orbit. The detectors and optics are designed to be as identical as possible, so images can be co-added to increase the gain.

The mast is not stiff enough in orbit to maintain the required alignment of the optics and detectors. To deal with this, a star camera, developed by DTU, and two metrology lasers are incorporated, which when combined can measure translation, tip, tilt and clocking between the two telescopes. The required corrections are made on the ground. Figure 4 shows a diagram of NuSTAR, (Harrison et al., 2013).

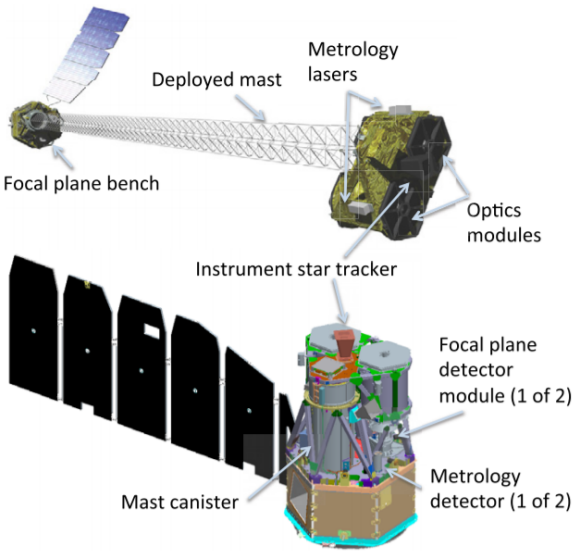

Figure 4: Diagram of NuSTARin the stowed (bottom) and deployed (top) configuration. Picture from (Harrison et al., 2013)

3.1 Instrument

Optics

Each of the two optics is made of 133 nested multilayer-coated shells. There are 89 inner shells, and 44 outer shells. The inner shells is comprised of 12 mirrors, while the outer is comprised of 24 mirrors. The mirrors are designed such that high energy photons graze the mirror and is focused into the detector panels. Usually X-rays are either absorbed or transmitted when the angle of inclination is high. For X-rays to be reflected the angle typically has to be $10'$ to $2°$, (Singh, 2005). The parameters of the optics are shown in Figure 5.

Optics Parameters

Optics Parameter	Value	Optics Parameter	Value
Focal length	10.14 m	Shell length	22.5 cm
No. of shells	133	Min. graze angle	1.34 mrad
No. of azimuthal segments	6 (inner)/12 (outer)	Max. graze angle	4.7 mrad
Inner radius	5.44 cm	Coatings (inner)	Pt/C
Outer radius	19.1 cm	Coatings (outer)	W/Si

Figure 5: The parameters of the optics. Taken from (Harrison et al., 2013)

The inner shells are coated with Pt/C multilayers which efficiently reflects below 78.4 keV, while the outer shells are coated with W/Si multilayers which reflect below 69.5 keV. The effective field of view of the optics decrease with the energy of the photons. At 10 keV the effective area is $10'$ and at 68 keV it is $6'$.

Focal planes

The focal planes consists of solid state CdZnTe pixel detectors surrounded by CsI anti-coincidence shields, (Harrison et al., 2013). The detectors are set in a 2×2 array, each with 32×32 pixels providing a $12'$ field of view. The on-board computer identifies the column and row of the largest pulse height, generated by a photon, and reads the pulse information of that pixel along with the pulse information of the neighbouring 8 pixels. The processing time of an event is 2.5 ms. A dead time will thus occur when there are many counts per second per pixel. By measuring the dead time and the pulse height NuSTARextrapolates the amount of events during the dead time, which will give an estimated of the actual intensity of the source it is looking at.

Aperture stops were deployed along with the mast post-launch to limit background noise. This is partially achieved, but some stray light still imping the detectors with energies below 10 keV. The parameters of the focal planes are given in figure 6.

Focal Plane Parameters

Focal Plane Parameter	Value	Focal Plane Parameter	Value
Pixel size	0.6 mm/12.″3	Max. processing rate	400 events s^{-1} $module^{-1}$
Focal plane size	$12' \times 12'$	Max. flux meas. rate	10^4 counts s^{-1}
Hybrid format	32 pix × 32 pix	Time resolution (relative)	2 μs
Energy threshold	2 keV	Dead time fraction (at threshold)	5%

Figure 6: The parameters of the focal planes. Taken from (Harrison et al., 2013)

Mast and metrology system

The mast is made of carbon fiber, aluminium and steel components, and is designed to be as isothermal as possible. Between night time and day time, the mast does however experience small deflection that results in motion of the optics and the X-ray focal point on the detectors. The deflection varies from 1 to 3 mm per orbit, which is enough for corrections to be made. The motion of the mast is tracked by two lasers on the optics that focuses down to a silicon detector near the focal planes. In combination of the star camera, accurate corrections of the position of the X-rays can be made on ground.

3.2 Data acquisition

NuSTARoutputs FITS-formatted data. The High Energy Archive Research Center (HEASARC) has created the FITS-file utility software necessary to produce high level scientific data products. The data processing is organized in the stages, (Forster et al., 2014):

1. **Stage 1 - Data calibrations:** Here data is processed for metrology, attitude corrections, flagging of hot/bad pixels, event reconstructions, energy calibrations, event flagging and coordinate transformation. The outcome is Level 1a calibrated event files.
2. **Stage 2 - Data screening:** Here data is screened for passages through the SAA, and the data type is determined. The data types available is:
   (a) 01: Good quality science data
   (b) 02: Earth occultation
   (c) 03: Slew
   (d) 04: SAA passage
   (e) 05: Calibration source in view
   (f) 06: Dubious attitude reconstruction

   where 01 data is prefered, but 06 data can be used in a pinch. A filter file is generated, used for data screening and Good Time Intervals (GTIs). Lastly, the dead time correction is made, and the temporal keywords are updated. The output is now Level 2 Cleaned Event files.
3. **Stage 3 - Product extraction:** Here the Level 3 scientific data is produced. The standard data processing is done with the script `nuproducts`. This stage also involves the generation of Ancillary Response File (ARF) and the Response Matrix File (RMF) which is used for spectral fitting with the program `XSPEC`.

The script `nupipeline` typically process data in stage 1 and 2, and then `nuproducts` is used for stage 3 separately. The pipeline for the NuSTARdata analysis software (NuSTARDAS) is shown in appendix A.

Once the data is ready for analysis, it is possible to get an image of the source. This is done with the software `ds9` which require event files. The image, along with a catalogue, can confirm that the source one is looking at, is in fact the bursting source, (Perri et al., 2016).

The light curves from the data products is suitable to perform time resolved spectral analysis on. `nuproducts` accepts a user specified GTI which allows bursts to be split into several intervals, usually in the form of rises, peaks and decays. The spectral analysis on each interval will be made using the program `XSPEC`. `XSPEC` can output the necessary parameters to characterize a LMXB. For this study, the interesting parameters during a burst will be:

1. **kT** : The color temperature of NS, measured in keV. As the NS bursts, the temperature is expected to initially rise, but fade back to normal values again as the burst ceases. For bursts exhibiting PRE, the temperature at the peak of the burst is expected to drop to maintain the Eddington luminosity, until it retracts to increase the temperature again.
2. **norm** : The norm is the bolometric luminosity at a distance of 10 kpc:
   $$\text{norm} = \frac{(R/1\text{ km})^2}{(d/10\text{ kpc})^2} \tag{22}$$
   from which the radius of the NS can be determined if d is known:
   $$R = \frac{d}{10}\sqrt{\text{norm}} \tag{23}$$
3. $\boldsymbol{\chi^2}$: The reduced χ^2 statistic will be shown along with the degrees of freedom (d.o.f) whose ratio should be close to 1. The closer to 1, the better the fit of the spectrum, the more reliable results of the other parameters.
4. $\boldsymbol{F}_{\text{abs}}$: The absorbed flux is measured in ergs cm^{-2} s^{-1}. During the X-rays journey from the NS to Earth, some of the flux has been absorbed in the interstellar medium. The flux is measured is in the energy band $2 - 100$ keV.

5. $\boldsymbol{F}_{\text{bol}}$: In order to find the flux from the NS before it has been absorbed in the interstellar medium, `XSPEC` uses a dummy response to extrapolate the bolometric flux from the limited F_{abs}[4].

Spectral analysis can also be performed on the persistent. If there is data for two consecutive bursts, all the necessary parameters in section 2.3 and 2.4 can be found using the measured F_{pers}.

In order to correctly track when bursts occur, NuSTARuses the NuSTAR time (NST). This is defined as the amount of second since January the 1$^{\text{st}}$ 2010 (UTC) known as the timezero. The time stamp can be decimal numbers. When an observation starts the timer starts at 0, so the actual time is: time+timezero. Data type 01 and 06 uses different timezeros, even within the same observation.

[4]The majority of photons emitted from a LMXB is in the energy band $2 - 80$ keV, but some fraction is outside this interval. By choosing $0.1 - 100$ keV it is expected to get almost the entire flux.

4 JEMX

The Joint European Monitor for X-rays (JEMX) is on board the INTEGRAL astronomical telescope, which was launched 2002 by ESA. Its orbit was initially 72 hours long, but was reduced in 2009 to 64 hours. The orbit is highly elliptical, (Kuulkers, 2015). JEMX fulfils three roles, (Chernyakova et al., 2015):

1. Aid IBIS and SPI[5] with complementary data at lower energies, and can track flux changes and spectral variability for aiding in interpretation of gamma data. Also helps with identification of sources in crowded fields.
2. Alert of new transients or unusual activity of known sources while scanning the galactic plane.
3. Deliver independent scientific results for sources in the field of view with soft spectra.

The third point is what makes JEMX suitable for detection of bursting neutron stars. JEMX consist of two nearly identical coded-aperture mask telescopes. Each unit, JEMX-1 and JEMX-2, is comprised of 3 subsystems: detector, its associated electronics and a coded mask. The instruments parameters are shown in Figure 7. In Figure 8 the overall design and the functional diagram is shown.

The energy range of JEMX is $3 - 30$ keV, which is narrower compared to NuSTARs range ($3 - 78$ keV). The spatial resolution is likewise topped by NuSTARs. However, the field of view ($5°$) of JEMX is much larger than that of NuSTAR (at best $10'$) making it a valuable asset for detecting sources of importance that would otherwise have been unnoticed.

Energy range	3 – 35 keV
Energy resolution†	$\Delta E/E = 0.40 \times [(1/E \text{ keV}) + (1/120 \text{ keV})]^{1/2}$
Field of view (diameter)‡	4.8° Fully illuminated 7.5° Half response 13.2° Zero response
Timing resolution	122 μs (relative timing) $\sim$ 1 ms (absolute timing)

† The energy resolution is slowly changing (degrading) over time.
‡ At the half response angle the sensitivity is reduced by a factor 2 relative to the on-axis sensitivity.

Figure 7: Table of JEM-X parameters. Some parameters insignificant to this study has been cut out. Picture from (Chernyakova et al., 2015)

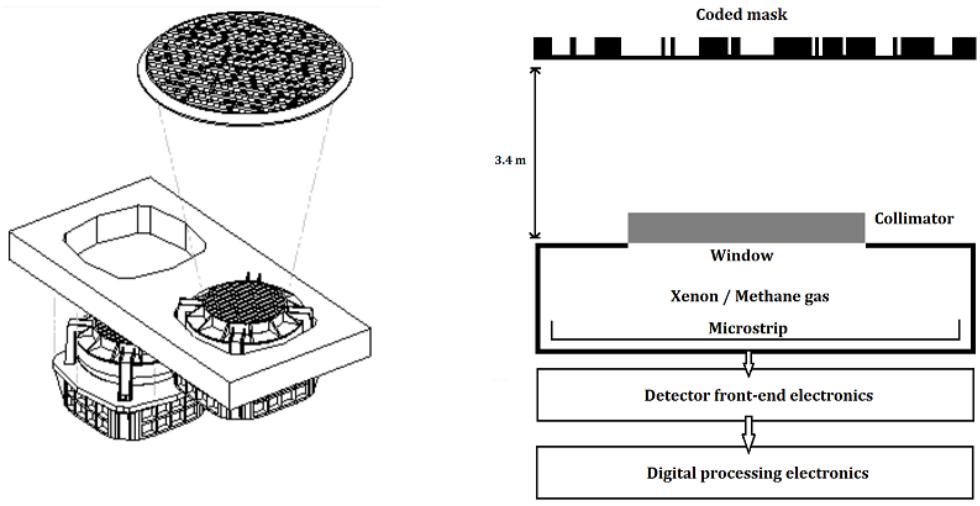

Figure 8: The functional design (left) and a reconstructed functional diagram of one unit (right). Picture from (Chernyakova et al., 2015) (original was of very poor quality)

[5]Imager on-Board the INTEGRAL Satellite and SPectrometer for INTEGRAL. Instruments for detection of gamma rays

4.1 Instrument

Detector

The detector is comprised of a microstrip in a gas chamber, with a mix of 90 % xenon and 10 % methan at 1.5 bar pressure. When a photon enters the chamber, its absorbed in the gas by photo-electric absorption releasing a ionization cloud which avalanches toward the strong electric field near the microstrips anodes. The electric charge is picked up as an electric impulse, and the position and location of charge is measured. Along with a timestamp, each event is given as a function of (x, y, t, E). The entire geometric sensitive area is 500 cm^2 per unit.

The window is a 250 μm thick beryllium foil which prevents the gas from escaping, while also allowing low-energy X-rays to pass through. Energies below 3 keV is blocked, setting the lower limit of detection of the instrument.

On top of the window is a collimator. It supports the window from the internal pressure, while significantly blocking the cosmic diffuse X-ray background from entering the detector. The collimator also defines the field of view of the detector. A negative side effect of the design is that sources near the edge of the field of view is attenuated, making data on the perimeter less defined. Radioactive sources in the collimator[6] with known energy outputs shines on well known parts of the microstrip. This allows the detector to be calibrated.

The anodes of the microstrip is eroding over time, reducing the sensitivity and the energy range. Despite this and INTEGRAL having exceeded its expected operation time and JEMX continues to produce useful scientific data.

Coded mask

The mask is based on a Hexagonal Uniformly Redundant Array. It uses a 25 % transparency mask, which provides a good sensitivity of complex fields with many sources. It is therefore well suited for observations of the Galactic plane and towards the center of the Galaxy, which is the primary location of LMXBs. The coded mask is positioned 3.4 m above the collimator.

When a photon enters through the coded mask and down to the detector, the resulting shadowgram[7] can via advanced mathematical formulas, connecting the area of the microstrip and the coded mask, reveal the position of the source on the sky. Figure 9 illustrates this.

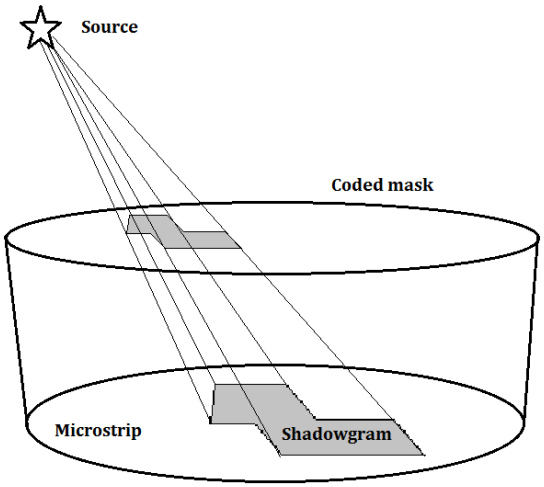

Figure 9: Illustration of the method to determine source location. The code on the mask is illustrative, the real code is hexagonal.

[6] $2\times^{55}$Fe and $2\times^{109}$Cd in JEM-X1. $4\times^{109}$Cd in JEM-X2.
[7] The pattern the ionization clouds from a specific source create.

4.2 Data acquisition

Data from JEMX comes in several formats. The most important telemetry format is the Full Imaging (FULL). The Restricted Imaging (REST) has poor time resolution, and is thus avoided. There exists other formats, but the FULL is the recommended one to use, and is what have been used for this study.

Data is being processed in a pipeline, much alike NuSTARs. The pipeline is split in 11 step, each processing the data differently, see Figure 10.

Tasks	Description
COR	Data Correction
GTI	Good Time definition and handling
DEAD	Dead Time derivation
CAT_I	Catalogue source selection for Imaging
BIN_I	Event binning for Imaging
IMA	Image reconstruction, source flux determination
SPE	Source spectra and response extraction (for XSPEC)
LCR	Source light curves extraction
BIN_S	Event binning for Spectral Analysis
BIN_T	Event binning for Timing Analysis
IMA2	Creation of mosaic images and summary on sources found

Figure 10: The pipeline used to produce scientific data from JEM-X

COR : Data is corrected for instrumental fingerprints and all pre-flight recorded anomalies that is known to be corrected for. Determination of transient problems is also done on this level.

GTI : Here the GTIs are defined. The GTIs are based on the satellite stability and data gaps due to lost packets in the telemetry flow. This results in intervals containing good data. The start up phase of the instrument may be included in the GTIs, though it hold significant errors the first few seconds.

DEAD : For every 8 seconds of data, the dead time is calculated, and the information is stored.

CAT_I : A list of known sources is selected, and a data structure containing known sources, their location and their expected flux is created.

BIN_I : This step defines the energy bins used for imaging within the GTIs and creates shadowgrams.

IMA : Here the sky images is created, and another scan for significant sources is performed. New additions are added with same data structure as in **BIN_I** with the addition of the information from the input catalogue.

SPE : The spectra of the individual sources found in **IMA** are extracted, and the ARF files needed for spectral fitting with `XSPEC` are generated.

LCR : The light curves for individual sources are generated.

The remaining steps are not used in this thesis. From the light curve, the program `lcurve` can fit a mathematical model to the decay of a burst using Equation (9), or by using mosaics generated from ESA software.

JEMX data is categorized in revolutions (around Earth), and each revolution contains a number of science windows. Each science window can be analysed separately, or combined to study the evolution of a bursting NS. The unit of time is INTEGRAL Julian Date (IJD) which is defined as JD[8] − 2451544.5, or MJD[9] − 51544, and is measured in days. The time stamp is expressed in TT, and not in UTC, like NuSTAR. When comparing the two instruments it thus important to take leap seconds into account.

[8] Julian Date is defined as days since January the 1st 4713 BC.
[9] Modified Julian Date is defined as days since January the 1st 2000.

4.3 Observation modes and types

INTEGRAL performs observations using three different modes. The standard observation mode is the rectangular dithering, which is also known as 5×5 dither. In this mode INTEGRAL points at 25 uniformly spaced point around the target position, see Figure 11. This mode allows for imaging with both IBIS, SPI and JEMX.

The second observation mode is the Hexagonal dithering. This mode compromises the image capabilities of IBIS and SPI, but JEMX is still able to produce data using this observation mode. In the hexagonal dithering INTEGRAL points at 6 points surrounding the target position, forming a hexagonal. This mode is suitable for single point sources.

The third and final observation mode is the staring mode. This seriously compromises imaging capabilities of IBIS, SPI and JEMX, so this mode is rarely used. Staring is usually used to point at the Crab which allows for calibration of the instruments on board.

INTEGRAL carries out 4 types of observation types. The normal, key programme and fixed time observations are the most frequent and easy to schedule observations. They may vary in the exposure time. The fourth observation type is the Target of Opportunity (ToO) type. This type is meant as a fast response to new phenomena, such as supernovae, AGN flares and outbursting X-ray sources.

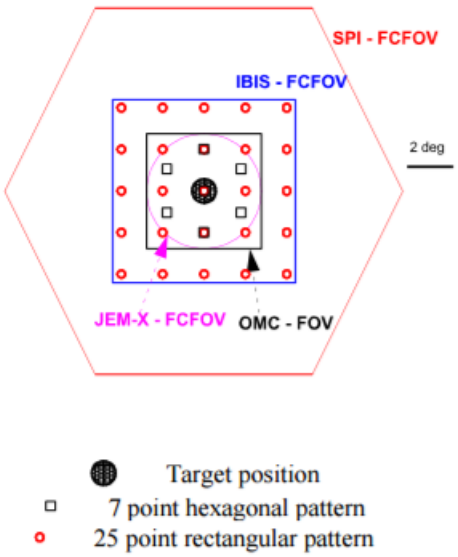

Figure 11: Schematic view of dithering pattern. Taken from (Kuulkers, 2015).

5 SAX J174853-202202

This study will focus on the X-ray source SAX J174853-202202. The source is a LMXB and has been observed in outburst by NuSTAR and INTEGRAL. NuSTAR has observed the source from February 26 2015 at 17:46:30.5 to February 27 2015 at 04:05:48.5. INTEGRAL has observed the source from Februray 18 2015 at 04:14:51.280 to March 24 2015 at 06:13:17.680[10]. The instruments have observed the same source within the same time period, so the hope is that a full, uninterrupted light curve can be constructed, which allows for more precise calculation of the various parameters and characteristics described in Section 2.

In this section the processing of data and results will be presented. First NuSTAR data will be analysed using `ds9`, `lcurve` and `XSPEC`. Afterwards INTEGRAL data will be analysed and finally a comparison of the results of the two instruments will be given.

5.1 NuSTAR

The event files of raw unprocessed data is opened with `ds9` to extract light curves and spectra. Using the event file holding data for SAX J174853-202202 (Henceforth abbreviated simply SAX), the image can be produced, see Figure 12. A catalogue has been added to include the name of the source. SAX one of a suspected 4-5 LMXBs that lie in globular cluster NGC 6440, which makes it difficult to establish the exact bursting object, (Galloway et al., 2008). Factoring in the many different name conventions, the source goes by many names. The exact location of the source is thus also difficult to establish, which explains that the position of the source is not exactly in the center of the bright region in Figure 12.

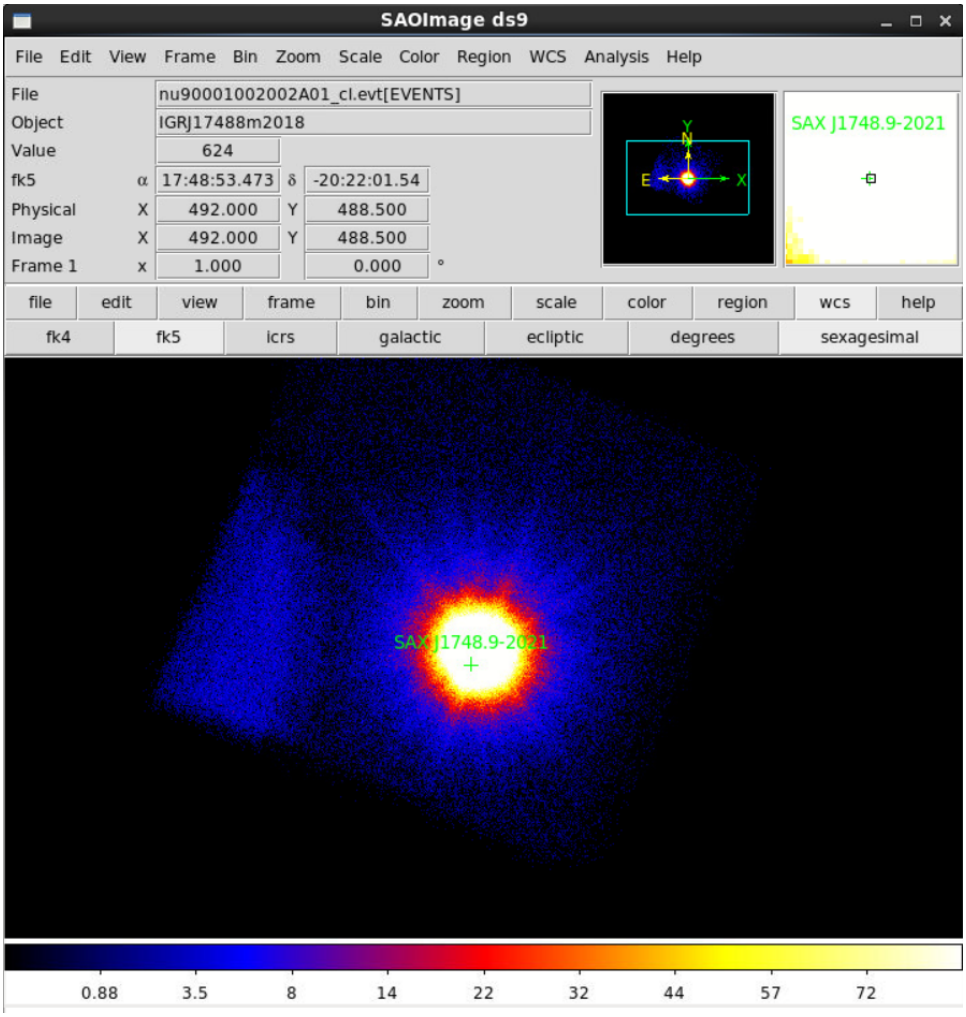

Figure 12: The image of SAX J174853-202202 using `ds9`.

[10] All times in UTC

When extracting the light curve of a source, its desired to remove the background noise from the space around the source that is interfering. This is done by selecting a region of seemingly no activity, extracting the light curves and spectrum, and subtract it from the sources light curve and spectrum.

`nuproducts` has been run for each focal plane module A and B (FPMA and FPMB) using both 01 and 06 data. Including the 06 data gives a few minutes extra of (dubious) data which may show a burst not detected by 01 data. `XSPEC` is able to do the spectral analysis of two light curves, why both A and B data is extracted to effectively double the count rate.

Figure 13 shows the entire light curve of SAX detected by FPMA using 01 and 06 data. The energy range is between channel 35 and 999, which is translates into energy expressed in keV through:

$$E[\text{keV}] = \text{channel} \times 0.04 + 1.6$$

The energy range is thus $3-42$ keV. The observation number is 90001002002. The observation is ~ 40000 seconds long, where data gaps, due to the revolution around Earth, are ~ 2200 s ≈ 37 min long. The accumulated data gap is ~ 13200 s $= 220$ minutes long, or approximately 25% of the observation.

The light curve shows 8 distinct bursts, where one is captured by the 06 data type. This emphasises the importance of including this data type to detect bursts. The bursts are numbered $1-8$ from left to right.

The lone data point after burst 4 is due to instrumentational error not caught in the data calibration and screening.

The light curve also show that only burst 3 and 4 has been observed consecutively. This allows the α to be determined using equation (8).

The recurrence time between bursts is shown in Table 1. As it is seen, the average recurrence time is ≈ 1.5 hours, which is not far from the estimates from (Galloway et al., 2008). The recurrence times are not very periodic, and one could expect that the data gap between burst 1 and 2 and 7 and 8 hides a burst. A spectral analysis revealing the accretion rate may help determine if bursts have been lost.

Burst	**1-2**	**2-3**	**3-4**	**4-5**	**5-6**	**6-7**	**7-8**	**Average**
$\boldsymbol{T_{\text{rec}}}$ **(min)**	117	66	36	88	114	62	122	86.4

Table 1: Recurrence time between bursts.

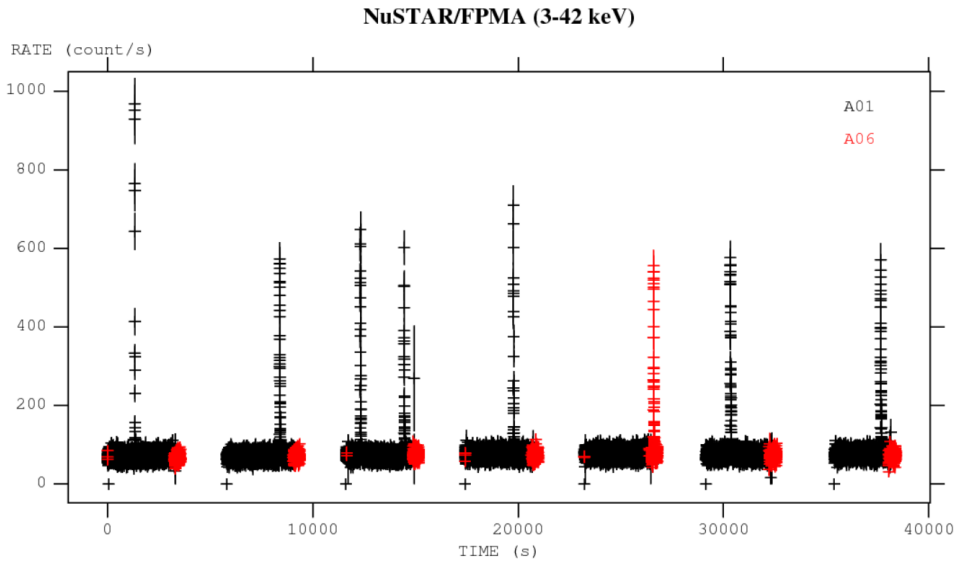

Figure 13: The light curve of SAX J174853-202202 using both A01 and A06 data.

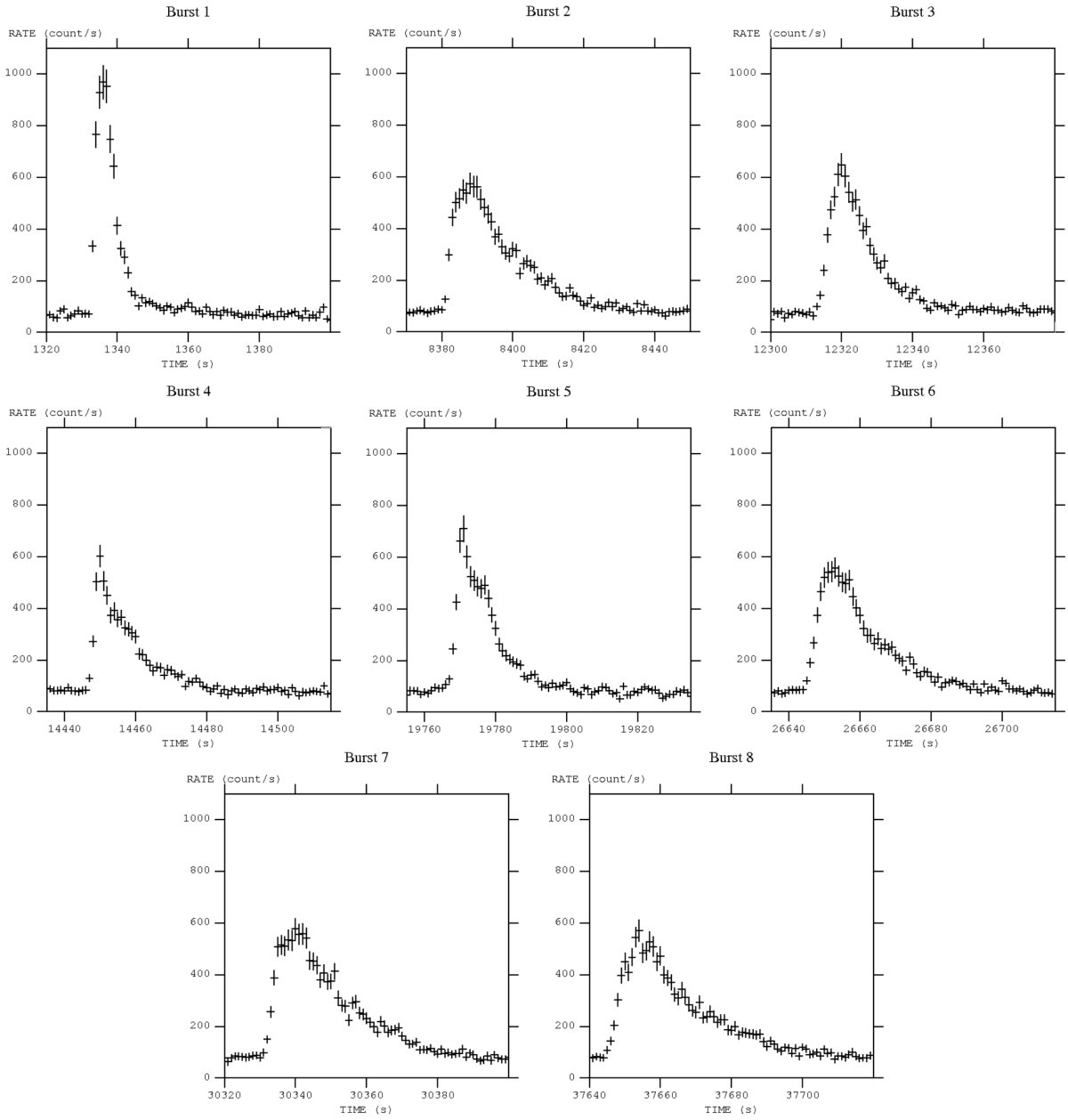

Figure 14: The light curves of the individual bursts.

Each individual burst is shown in Figure 14. The light curves are all scaled from 0 to 1100 on the y axis, and all show 80 seconds. This allow for easier comparison of the bursts.

When comparing the burst, the following intervals are used to describe a burst[11]:

- Rise : The rise of a burst is defined as the interval where the count rate has reached 25% of the peak count rate to about 90% of the curve peak. Rise is usually between 1 and 6 seconds, depending on the type of bursts.
- Peak : The interval around the peak of the curve. Peak is usually between 1 and 4 seconds, depending on the type of burst.
- Decay : The decay is the interval describing the tail from the peak to where the count rate reaches 25% of the peak count rate. The decay can last tenth to hundredth of seconds, even hours under rare circumstances.

[11]This convention is widely accepted, used by e.g. Chenevez (2010).

As described in section 2.4, the accretion rate should influence the type of burst that occurs. Burst 1 has a very steep rise, short peak, and steep decay. It would appear that the burst is a helium flash.

Burst 3, 4 and 5 has sharp peaks, while burst 2, 6, 7 and 8 has more round peaks. The decay times are the longest for burst 2, 6, 7 and 8, hinting at accretion rates between 0.1 and 1.0 of $\dot{m}_{\mathrm{Edd}}$. None of the burst lasts longer than 100 seconds, which suggest that the accretion rate did not go under 0.01 of $\dot{m}_{\mathrm{Edd}}$ during the observation period.

Another detail to burst 4, 5 and somewhat 6 and 7, is the bulge in the decay regime, a few seconds after the peak. The reason for the apparent "second" peak is not well understood, but possible explanations will be given in the discussion, Section 6.

When the light curve is produced, the resulting curve that is seen is the sum of the persistent and the burst. So in order to see the burst alone, the persistent has to be subtracted. `XSPEC` can do this when supplied with a spectrum of the persistent. A GTI needs to be constructed containing the interval between the burst that needs to be analysed, and the burst before it. Alternatively, if the persistent is at a constant level throughout the observation period, the entire observation can be used as the persistent. This either requires the bursts to be removed from the GTI, or to accept the small margin of error that the bursts introduces. The bursts last all together a maximum[12] of $8 \times 80 = 640$ seconds of high count rates, which compared to the total observation period of ~ 40000 is only $\lesssim 2\%$, so the error wont be large.

Still, an analysis of the persistent light curve without bursts is chosen, and is shown in Figure 15. The light curve has been rebinned to a 60 second bin time, using `lcurve`, as the 1 second bin time contained too many data points, making it impossible to see variations. The light curve show a small variation in the average count rate, starting from ≈ 71 c/s to ≈ 76 in the end of the observation. Thus it is chosen to find the persistent before each individual burst.

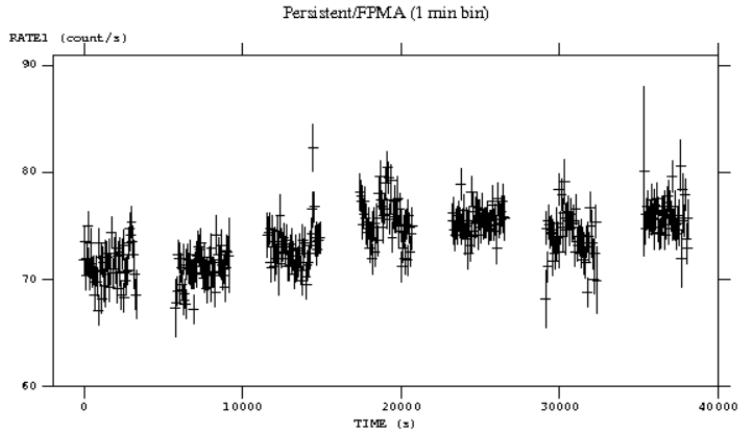

Figure 15: The light curve of the persistent (no bursts) with a 1 minute bin time.

When performing the time resolved spectral analysis using `XSPEC`, each burst is categorised in rise, peak and decay intervals, as previously defined. Each burst may have several rise, peak and decay intervals since each interval need to hold the same amount of counts $\pm 10\%$ of the counts per interval (c/I) chosen. When the c/I has been chosen, the bursts has been plotted in a graphing tool[13] which integrates, and finds the area under the trapeze formed by connecting each data point, see Figure 16. This method ensures a very precise estimate of the counts in each interval.

In Table 2 each burst is listed with the chosen c/I, the counts per second at the peak and the amount of rise, peak and decay intervals the chosen c/I has resulted in. When the intervals has been chosen, keeping the c/I within $\pm 10\%$ of the peak value has weighed higher than staying within the 25% and 90% thresholds mentioned earlier. This choice have been made to make sure that the spectral analysis of each interval gets approximately the same amounts of spectral data counts. The final decay interval typically have more than $\pm 10\%$ c/I, since it does not make sense to start another decay interval if the c/s will drop far below the 75% of the peak value, where the picked up counts might as well be from the persistent or noise.

[12] Assuming each burst lasting 80 seconds.
[13] Graph. Open source. Download at: `https://www.padowan.dk/download/`.

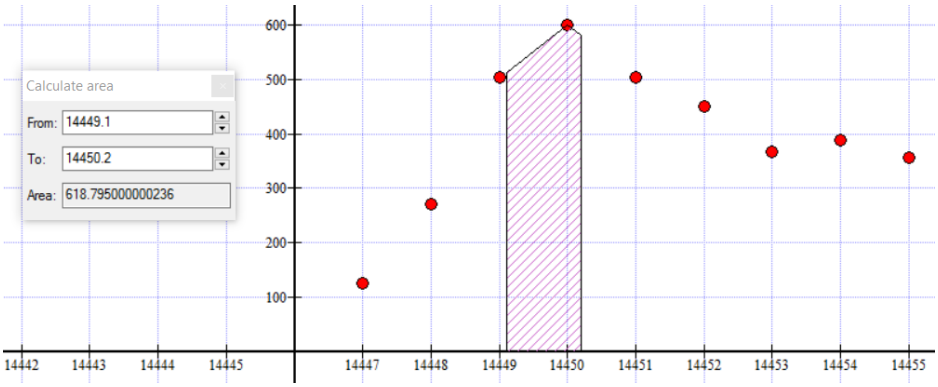

Figure 16: The graphing tool calculates the area under the data points, which yields the counts per interval. Shown in the figure is burst 4 with a c/I = 600.

Burst #	c/I	Rise #	Peak #	Decay #	∼Peak (c/s)
Burst 1	1000	2	2	2	950
Burst 2	1000	2	2	7	570
Burst 3	1000	2	1	5	600
Burst 4	600	1	1	8	600
Burst 5	800	1	2	6	700
Burst 6	1000	2	2	6	550
Burst 7	1000	1	4	8	575
Burst 8	1000	2	3	8	575

Table 2: Table of the chosen c/I, number of rise, peak and decay intervals and the peak of each burst.

5.1.1 Spectral analysis

`XSPEC` is used to perform the time resolved spectral analysis that can produce the parameters mentioned in Section 3.2, making it possible to see the time evolution of the parameters of the NS.

`XSPEC` requires the .pha file for the interval (rise, peak etc.) and the .pha background file from the persistent. Both were obtained running `nuproducts`. `XSPEC` tries to fit the spectrum with a model that the user provide. Multiple models can be assigned, and the user gives the best estimate of the parameters of the model. `XSPEC` then fits the data using an iterative process that modifies the parameters until the statistic χ is minimized. Parameters that are thought to be constant can be kept frozen, making the process faster, and preventing `XSPEC` to fit a model using parameters that are non physical/wrong.

To take into account the absorption of photons in the interstellar medium, the absorption model `TBabs` is used, whose parameter n_{H} is the equivalent hydrogen column expressed in units of 10^{22} atoms cm^{-2}. The parameter is set to 0.82 and is kept frozen, (Chenevez, a).

When `XSPEC` has fitted a model to the spectrum, the temperature, norm and absorbed flux is determined with error intervals. The χ statistic along with the d.o.f is also displayed. The ratio of χ and d.o.f gives the reduced χ_{R} which must be close to 1 in order for the fit the be good.

The bolometric flux[14] can be found using the `dummyrsp` command, which create a dummy response matrix with which the model can be examined outside the data's energy response[15]. The selected range of the bolometric flux is $0.1 - 100$. In this range very little flux is estimated to be lost.

[14] The corresponding flux of photons of all energies.
[15] Source: (Arnaud et al., 2017).

	Burst 1	**Burst 2**	**Burst 3**	**Burst 4**	**Burst 5**
$\boldsymbol{\chi}_{\mathrm{R}}$	$\frac{1770.01}{1842} = 0.958$	$\frac{1800.12}{1842} = 0.977$	$\frac{1528.27}{1842} = 0.830$	$\frac{1912.33}{1842} = 1.038$	$\frac{1818.76}{1842} = 0.987$
$\boldsymbol{F}_{\mathrm{abs}}$	3.0699 ± 0.0124	3.0629 ± 0.0114	3.117 ± 0.025	3.110 ± 0.0121	3.261 ± 0.0125
$\boldsymbol{F}_{\mathrm{bol}}$	10.97 ± 0.044	11.25 ± 0.042	12.71 ± 0.1	12.276 ± 0.048	13.044 ± 0.05
	Burst 6	**Burst 7**	**Burst 8**	**All persistent**	
$\boldsymbol{\chi}_{\mathbf{R}}$	$\frac{1928.14}{1842} = 1.047$	$\frac{1675.89}{1842} = 0.91$	$\frac{1846.88}{1842} = 1.002$	$\frac{2602.27}{1842} = 1.413$	
$\boldsymbol{F}_{\mathbf{abs}}$	3.224 ± 0.0088	3.177 ± 0.0155	3.234 ± 0.011	3.180 ± 0.0036	
$\boldsymbol{F}_{\mathbf{bol}}$	12.523 ± 0.034	12.201 ± 0.06	12.49 ± 0.043	12.183 ± 0.0138	

Table 3: Table of the absorbed and unabsorbed bolometric flux along with the reduced χ statistic for all the persistent accretion before the burst specified. All fluxes are in unit of 10^{-9} ergs cm^{-2} s^{-1}. Even though burst 6 was caught with the 06 data type, the persistent flux is calculated from the more abundant 01 data before the burst.

The downside of using a dummy response is the loss of error intervals. Two methods can be used to estimate the errors. First, the flux is dependent on the distance and luminosity of the NS, and so the error intervals can be found by applying the errors of these onto the flux. The second method is to assume that the ratio of F_{abs} and F_{bol} can be applied to the errors of F_{abs} to give the errors of F_{bol}:

$$\delta F_{\mathrm{bol}} = \frac{F_{\mathrm{bol}}}{F_{\mathrm{abs}}} \delta F_{\mathrm{abs}}$$

The latter method will be used in this study.

Persistent

The model used to fit the persistent was initially a pure black body radiation (`bbodyrad`), also used to describe the bursts, but the χ_{R} statistics were extremely poor, and thus it was chosen to use the broken power law `bkn2pow`, which included 2 break energies. The results of the analysis can be seen in Table 3. The error margin of the absorbed flux is not symmetric, but the difference between the upper and lower error margin was typically $\lesssim 0.5\%$ of the greater of the two, so it was chosen to find average of the two and list that value.

From the table it is seen that the χ_{R} for the individual bursts are quite close to 1, with the exception of the accretion before burst 3, whose $\chi_{\mathrm{R}} = 0.83$. With the amount of d.o.f this value should be higher. The explanation is likely found in the exposure time. In Figure 13 it is seen that burst 3 start relatively after a data gap, reducing the amount of seconds that `XSPEC` could fit data to.

The χ_{R} of the total persistent (without bursts) is not very close to 1, considering the d.o.f. This hints that the model used does not give a good explanation of the persistent. The bolometric flux is seen to be ≈ 4 times higher than the absorbed flux. The expected bolometric flux is not expected to be of this magnitude which further questions the model, (Chenevez, a). The source's radiation will fall at very low and very high energies, which are the ones that are being extrapolated. The broken power does give good χ_{R} statistics, but it is not very well suited to give a physical explanation of the data.

To avoid reproducing the data using a new model, a correction factor that can be applied to the bolometric flux can be determined. Using the data from the entire persistent (without bursts), a new model can be fitted to the persistent which gives a better physical explanation to the persistent phenomena.

The new model includes the `diskbb` which gives the spectrum of an accretion disc consisting of multiple black body components, (Arnaud et al., 2017). Comptonization, described in Section 2, likely occurs around the NS, and has to be accounted for as well. Thus the model `compTT` is applied as well to account for comptonization. The two models `diskbb+compTT` are used with `XSPEC` to find the bolometric flux with the following parameters:

	Burst 1	**Burst 2**	**Burst 3**	**Burst 4**	**Burst 5**
$\boldsymbol{\chi}_{\mathrm{R}}$	$\frac{1770.01}{1842} = 0.958$	$\frac{1800.12}{1842} = 0.977$	$\frac{1528.27}{1842} = 0.830$	$\frac{1912.33}{1842} = 1.038$	$\frac{1818.76}{1842} = 0.987$
$\boldsymbol{F}_{\mathrm{abs}}$	3.0699 ± 0.0124	3.0629 ± 0.0114	3.117 ± 0.025	3.110 ± 0.0121	3.261 ± 0.0125
$\boldsymbol{F}_{\mathrm{bol}}$	4.212 ± 0.017	4.320 ± 0.016	4.87 ± 0.038	4.713 ± 0.0184	5.008 ± 0.0192
	Burst 6	**Burst 7**	**Burst 8**	**All persistent**	
$\boldsymbol{\chi}_{\mathbf{R}}$	$\frac{1928.14}{1842} = 1.047$	$\frac{1675.89}{1842} = 0.91$	$\frac{1846.88}{1842} = 1.002$	$\frac{2602.27}{1842} = 1.413$	
$\boldsymbol{F}_{\mathbf{abs}}$	3.224 ± 0.0088	3.177 ± 0.0155	3.234 ± 0.011	3.180 ± 0.0036	
$\boldsymbol{F}_{\mathbf{bol}}$	4.808 ± 0.013	4.684 ± 0.023	4.795 ± 0.0165	4.677 ± 0.0005	

Table 4: Table of the absorbed and unabsorbed bolometric flux along with the reduced χ statistic for all the persistent accretion before the burst specified. All fluxes are in unit of 10^{-9} ergs cm^{-2} s^{-1}. The bolometric fluxes have been corrected with the correction factor X_{corr}.

- `TBabs`: $n_H = 0.82$ (frozen)
- `diskbb`: $T_{\mathrm{in}} = 2.7$
- `compTT`: Redshift $= 0$ (frozen upon fitting)
- `compTT`: $T_0 = 0.4$
- `compTT`: $k_T = 5$
- `compTT`: $\tau_p = 2.5$

The remaining parameters were left empty for `XSPEC` to find. The found bolometric flux with the new model was:

$$F_{\mathrm{bol,diskbb+compTT}} = 4.677 \times 10^{-9}\,\mathrm{ergs\ cm^{-2}\ s^{-1}}$$

Using the ratio between $F_{\mathrm{bol,diskbb+compTT}}$ and $F_{\mathrm{bol,bkn2po}}$, found in table 3, yields the correction factor:

$$X_{\mathrm{corr}} = \frac{F_{\mathrm{bol,diskbb+compTT}}}{F_{\mathrm{bol,bkn2po}}} = \frac{4.677 \times 10^{-9}}{12.183 \times 10^{-9}} = 0.384$$

This factor can be applied to the bolometric fluxes found in Table 3 to find the more correct estimates of the bolometric flux. Table 4 is the updated version of Table 3 with X_{corr} applied to the bolometric fluxes.

In Figure 17 the normalization plot for both the fit of `bkn2po` and `diskbb+compTT` is shown beside each other. In the top panels it shows the data (black) and the fit (red). It is seen that the count rate is reduced at higher energies. In the lower panel the ratio of the two is shown, which obviously should be as close to 1 to have a good fit. The left plot shows the new model with `diskbb+compTT` which is seen to provide a better fit in the higher energies due to `compTT`, while also staying more stably around the ratio of 1. The right plot shows the old model `bkn2po` which 'wobbles' up and down even in the lower energies. At high energies this model fails to provide a good fit. The energy range was set to 3 to 30 keV, since higher energies was poorly fitted by `XSPEC`, and it could be argued, that the count rate is very low at these energies ($\lesssim 0.01$), justifying this choice.

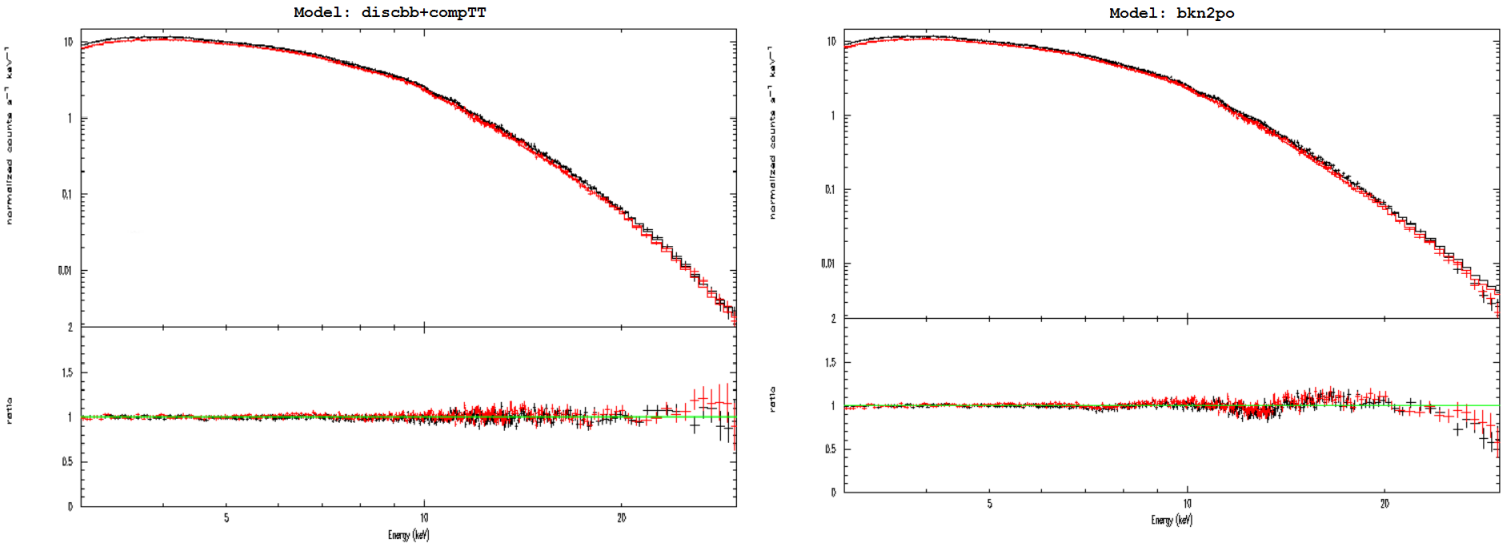

Figure 17: The normalization plot of both models.

Bursts

The bursts was modelled with the black body model `bbodyrad`. Each burst has been categorised intervals as shown in Table 2. The time resolved spectral analysis is shown in Figure 18 and 19.

As it turned out, the χ_{R} statistic for the fit of burst 6 was very poor (~ 0.6) resulting in error intervals spanning up to 30 times the predicted values. It was thus chosen to exclude this plot as the data was simply nonsensical.

The first panel shows the bolometric flux as time progresses during a burst. All bursts are seen to have a rise in bolometric flux during the peak of the burst. Burst 1 is seen to reach the highest bolometric flux, with a peak at $F_{\mathrm{bol}} \approx 3.4 \times 10^{-8}$.

The second panel shows the color temperature at the surface, expressed in keV. Most bursts sees a clear rise in temperature during the peak, while falling during the decay period. Most bursts reaches temperatures of $\sim$ 2.5 keV and drops to $\sim$ 1.8 keV at the end of the burst. keV is translated into a temperature via[16]:

$$T(\mathrm{Kelvin}) \sim 1.16 \times 10^7\, T(\mathrm{keV})$$

which corresponds to temperatures of $\approx$ 30 million Kelvins at the peaks, and $\approx$ 20 million Kelvins at the end of a burst.

The third panel shows the black body radii of the NS during a burst. All bursts are seen have very undefined black body radii, that are impossible to deduce anything sensible from. It is thought to be a result of the bad χ statistic, where the error margin are propagated in R^2, which yields the large error margins of R_{bb} compared to f_{bol} and kT_{bb}. The black body radii has been calculated assuming $d = 8.1$ kpc, inferred from (Galloway et al., 2008).

The fourth panel shows the χ_{R} statistics for each interval during a burst. Black cross markings has been applied for visual aid. Nothing general can be said about χ, although it appears that in burst 2, 4, 5, 6 and 7 it came close to 1 during the peak of a bursts, and then dipped immediately afterwards. During the peak the counts per second is at its highest, resulting in more spectral data counts, which may explain the good χ.

[16] Source: (Formulas, 2012)

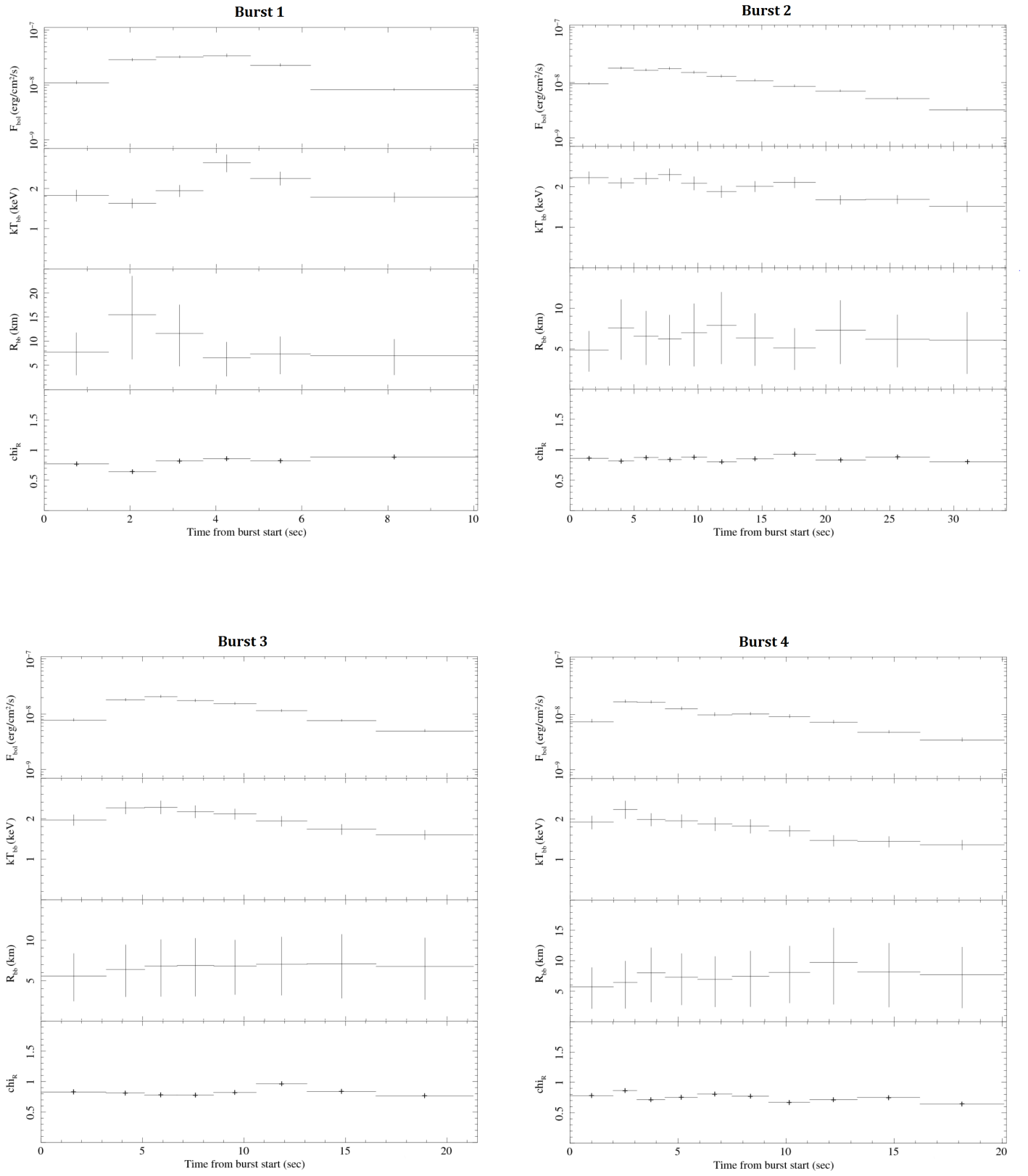

Figure 18: Time resolved spectral analysis of burst 1 to 4.

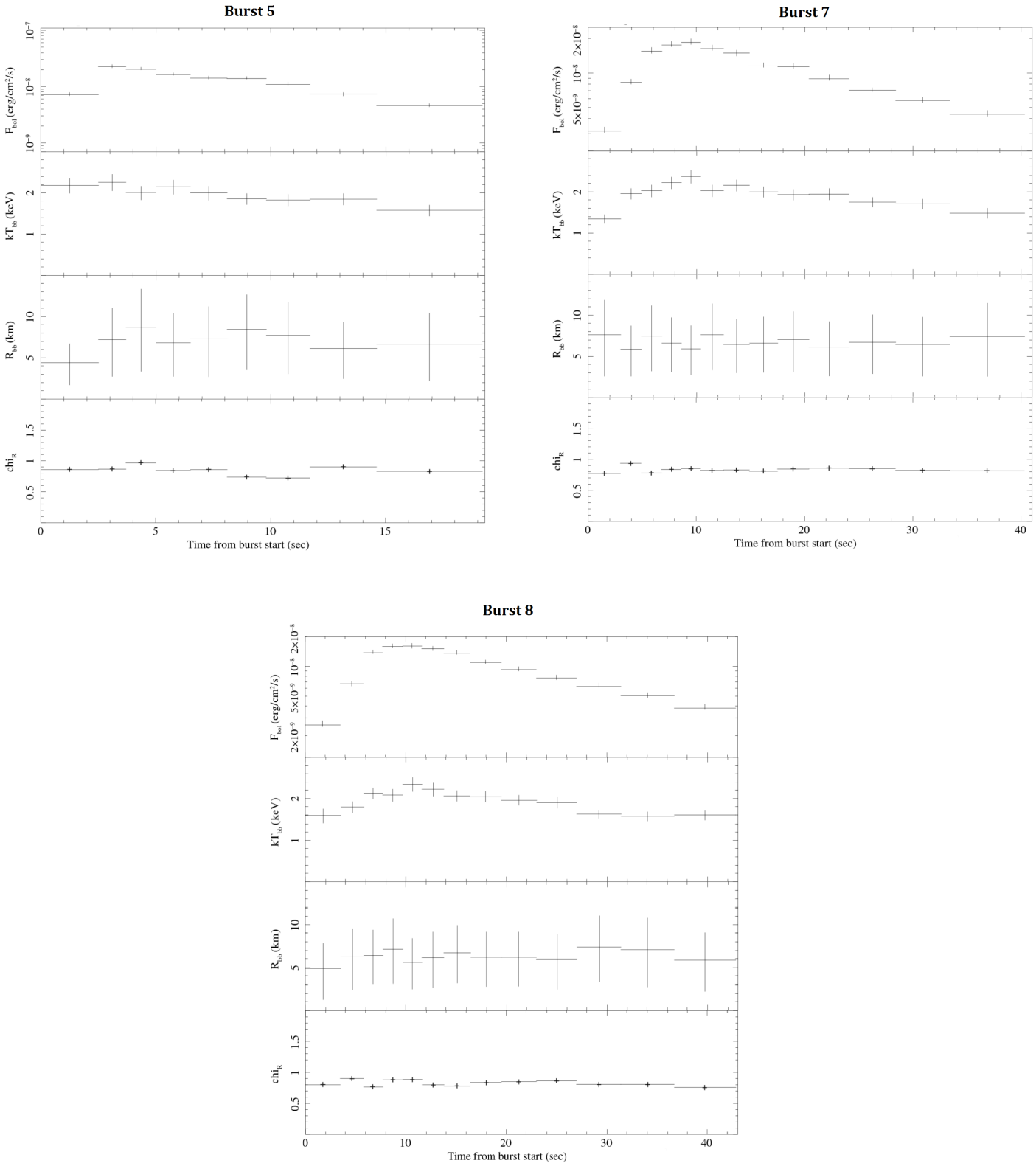

Figure 19: Time resolved spectral analysis of burst 5 to 8.

Burst 1 was suspected to be a helium flash, which the plot verifies. From the plot it is seen that the temperature initially dips, while the flux remains constant. The radius of the NS during burst 1 is the best defined (least worst) and to some extend its possible to see that the radius increases during the peak. This anti-correlation of radius and temperature, along with the constant flux, indicates a photospheric radius expansion, (Galloway et al., 2008), where the flux has reached the Eddington luminosity limit. In order to maintain the luminosity, the temperature must drop, while the radius expand. The peak luminosity for burst 1 was $F_{\text{bol}} \approx 3.418 \times 10^{-8}$ ergs cm^{-2} s^{-1} which through Equation (10) translates into a local Eddington luminosity limit of:

$$L_{\text{Edd}} = 4\,\pi\,d^2 \cdot 3.418 \times 10^{-9} = 2.68 \pm 1.036 \times 10^{38}\,\text{ergs s}^{-1} \tag{24}$$

which is not far from the estimates of Galloway et al. (2008) and Kuulkers et al. (2003). d is assumed 8.1 kpc and has been assigned an error of ± 1.3 kpc, (Galloway et al., 2008).

The spectral data counts for each interval was generally about half of the amount of counts that were found be integrating under the curve. The spectral analysis was performed on the dead time corrected data, and thus it was chosen to attempt to improve the radii determinations by choosing the original data set, called RATE_ORIG, which has not been dead time corrected. This was tested on burst 2. The c/I was initially chosen to be 1000, which would give fewer intervals since the count rate is lower in the RATE_ORIG data set.

The resulting estimates of the radius turned out to have smaller error margins, but it was still not possible to say anything about the evolution of the it. Also, the intervals became so long, that variations throughout a burst would be lost. To avoid loosing variations, it was chosen to try 500 c/I. This made variations a little clearer, but the error margins was still too great to conclude anything. Both the 500 and 1000 c/I yielded a better χ statistic, but it was deemed that the small increase in χ did not justify spending time on performing the entire time resolved spectral analysis for all bursts again. The spectral analysis of the three cases is shown in Figure 20.

It is worth noting that the spectral data count was matched with the c/I with a 99% accuracy using the RATE_ORIG data, verifying that the method of counting counts per interval is precise. Halving and doubling the data counts of the standard data was also attempted to see, if the large error margins was caused by large variation. This caused larger errors on shorter intervals and smaller errors on longer, so the cause of large errors was not high variation on short time scales.

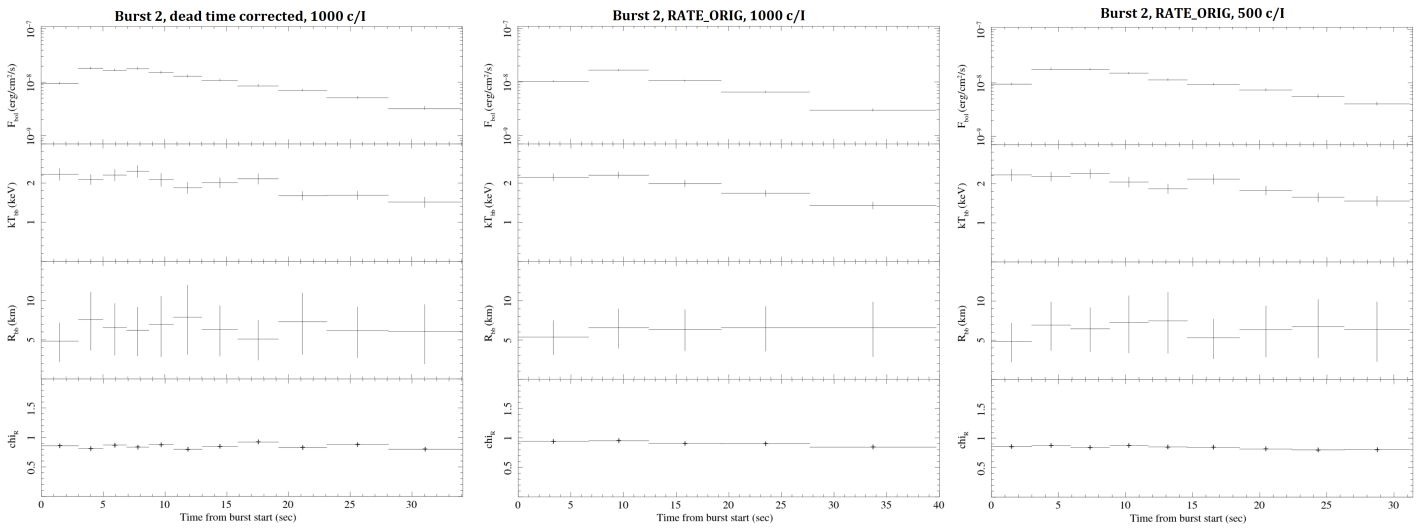

Figure 20: Time resolved spectral analysis of burst 2. Left panels: Analysis using deadtime corrected data, using 1000 c/I. Middle panel: Analysis using the original count rates, using 1000 c/I. Right panels: Analysis using the original count rates, using 500 c/I.

To compute the α parameter, used to determine various other parameters described in Section 2, two consecutive bursts need to be observed. Burst 3 and 4 was the only two consecutive bursts that was observed in this observation. This makes it possible to determine α for burst 4 through Equation (8). The fluence $E_{\rm b}$ is found be multiplying the bolometric flux of each interval with the intervals time length, summing up all interval fluences. The persistent is found in Table 4. The recurrence time is found in Table 1. This yields:

$$\alpha = 60.81 \pm 12.92$$

No error has been assigned to the time $t_{\rm rec}$.

The found α suggest a mixed H/He burning trigged by unstable helium ignition. The accretion rate is expected to be in the range of $0.1 - 1.0$ of $\dot{m}_{\rm Edd}$. The accretion rate is found using equation (15):

$$\dot{m} = 14880 \pm 4834 \text{ g cm}^{-2} \text{ s}^{-1}$$

Where the radius is assumed 12 km with no errors, and a gravitional redshift of $z + 1 = 1.31$.

The local Eddington accretion rate is found using the luminosity Eddington limit found in Equation (24) using Equations (6) and (7) in combination:

$$\dot{M}_{\rm Edd} = \frac{2.68 \times 10^{38}}{\eta\, c^2} = 1.492 \pm 0.58 \times 10^{18} \text{ g s}^{-1}$$

$$\dot{m}_{\rm Edd} = \frac{1.594 \times 10^{18}}{4\,\pi\, R^2} = 82426 \pm 31799 \text{ g cm}^{-2} \text{ s}^{-1}$$

which gives the ratio:

$$\frac{\dot{m}}{\dot{m}_{\rm Edd}} = 0.181$$

which is in accordance with the found α. Using the found accretion rate, the ignition column depth, and thus the total mass burned, can be found using Equation (16) and (17):

$$y = 2.454 \pm 0.798 \times 10^{7} \text{ g cm}^{-2}$$

$$M_{\rm b} = 4.44 \pm 1.44 \times 10^{20} \text{ g}$$

Using α, the energy efficiency can be found via Equation (19):

$$\varepsilon = 3.3 \pm 0.7 \times 10^{18} \text{ erg g}^{-1}$$

where the ratio of the isotropy factor of the burst and persistent has been assumed $\xi_b/\xi_p = 0.85$, (Chenevez, b). The total energy released during burst 4 is now found using Equation (20):

$$E_{\rm b,rel} = 1.117 \pm 0.6 \times 10^{39} \text{ ergs}$$

The composition of the burst is ready to be determined using Equation (21):

$$X \approx 0.42$$

Thus the burst consisted of $\sim 42\%$ hydrogen and $\sim 58\%$ helium, which is in agreement with the mixed H/He burning that was predicted.

Another way of finding α is using Equation (9) to find the fluence of the burst using the decay time constant τ which can be found using `lcurve` that can fit an exponential decay to the burst. The model `BURS` takes 4 inputs; Start time of the burst, the peak time of the burst, a guess of the decay time and the peak count rate. A constant will be added to the model so that the decay settles at the persistent level. The decay time `DT` is guessed at 10 s, the peak count rate `BN` at 650 c/s and the constant `CO` at 70 counts. The model is fitted and the inferred τ is determined. In Figure 21 the fit is shown, along with the inferred parameters to the right of the plot.

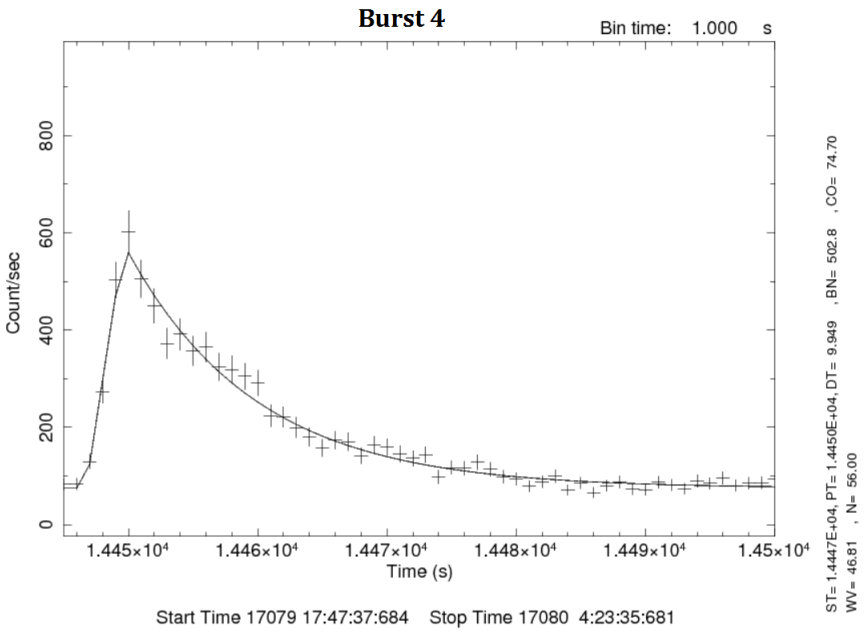

Figure 21: The fit of exponential decay to burst 4.

With the found τ, the fluence of the burst can be found using the peak flux of $F_{\text{peak}} = 1.699 \times 10^{-8}$ ergs cm^{-2} s^{-1}:

$$E_{\text{b}} = 1.465 \pm 0.079 \times 10^{-7}$$

which yields the α:

$$\alpha = 69.49 \pm 3.75$$

The α found using this method differs from the found α using the first method. α fortunately fits well into the error thresholds. The second method yields better error margins since τ has not been assigned any error. The first method sums up all fluence for each interval which increase the error of the total fluence to $\sim 20\%$, while the second methods only has an error of the fluence of $\sim 5\%$.

Table 5 show the estimated accretion rates calculated from Equation (15) using the fluxes from Table 4. By assuming no bursts has been lost in the data gaps, the α parameters has been determined, and from that the composition of the bursts has been established.

The composition of burst 5 appeared negative, which implies that the persistent fluence is incorrect, which might be because that a burst have been missed in a data gap between burst 4 and 5. Burst 5's α is also much higher than the others, which is an effect of the wrongly determined persistent fluence. Had a burst occurred in the data gap, $t_{\text{rec}} \approx 3800$ s, which would have resulted in a $\alpha \approx 90$, which would fit better into the other α's of the other bursts. This would give a composition of $X \approx 0.13$. The hydrogen amount has doubled from burst 2 to 3, and again from burst 3 to 4. The two undetermined values unfortunately conceals to evolution of this trend, but burst 7 is seen to have even higher amounts of hydrogen than burst 4. Then on burst 8 a significant decrease in X is seen. There is a data gap between burst 7 and 8 which could be hidden here, that would bridge the large gap in X.

Interesting is it to see that the accretion rate is above 0.1 of $\dot{m}_{\text{Edd}}$ before burst 1. According to the theory, the accretion rate should be between 0.01 and 0.1 of $\dot{m}_{\text{Edd}}$ in order for a helium flash to occur. But nonetheless, the time resolved spectral analysis of burst 1 quite clearly revealed a photospheric radius expansion, which is common in helium flashes. The duration of the burst also suggests a helium flash.

Burst 6's data is not very reliable, as the peak bolometric flux is ≈ 50 times lower than the other bursts. The accretion rate however, is determined from 01 data, and should thus be reliable.

	$\dot{m}$	$\dot{m}/\dot{m}_{\mathrm{Edd}}$	$F_{\mathrm{b,peak}}$	E_{b}	α	X	Δt
Burst 1	1.3298 ± 0.432	0.161	34.184 ± 2.216	1.844 ± 0.259	-	-	10.1
Burst 2	1.364 ± 0.43	0.165	18.177 ± 0.891	3.206 ± 0.54	94.61 ± 16.26	0.13	34
Burst 3	1.5376 ± 0.506	0.187	20.729 ± 1.107	2.351 ± 0.34	82.03 ± 12.5	0.21	21.3
Burst 4	1.4880 ± 0.483	0.181	16.988 ± 0.914	1.674 ± 0.349	60.81 ± 12.91	0.42	20.1
Burst 5	1.5811 ± 0.514	0.192	22.452 ± 1.437	2.052 ± 0.378	128.82 ± 24.23	NaN	19.2
Burst 6	1.5180 ± 0.491	0.184	0.747 ± 0.389	0.183 ± 0.329	1798.3 ± 3238.4	NaN	31.1
Burst 7	1.4789 ± 0.482	0.179	18.42 ± 1.043	3.75 ± 0.73	46.46 ± 9.28	0.68	40.3
Burst 8	1.5139 ± 0.491	0.184	16.094 ± 0.952	3.568 ± 0.685	98.37 ± 19.23	0.11	42.8

Table 5: $\dot{m}$ is measured in units of 10^4 g cm^{-2} s^{-1}. $\dot{m}_{\mathrm{Edd}}$ is the one found in equation (5.1.1). $F_{\mathrm{b,peak}}$ is the peak bolometric flux measured during a burst, and is measured in units of 10^{-9} ergs cm^{-2} s^{-1}. E_{b} is the burst fluence, and is measured in units of 10^{-7} ergs cm^{-2}. X specifies the H/He ratio of the burst, where $X = 1$ is pure hydrogen. Δt is the bursts duration.

The found bolometric peak fluxes is very consistent with the ones found in Galloway et al. (2008). So is the recurrence times. In Figure 22 a visual representation of data has been carried out. From it, no clear correlation between any of the parameters can be seen. Like mentioned in Galloway et al. (2008), no correlation between the persistent flux and burst duration was seen. However, unlike Galloway et al. (2008), the α did not appear to be strongly anti-correlated with burst duration. A slight anti correlation might be seen between the burst duration and bolometric peak flux. It should be clearly stated that the $y - axis$ holds no real value and that the plot is only for visualising variations.

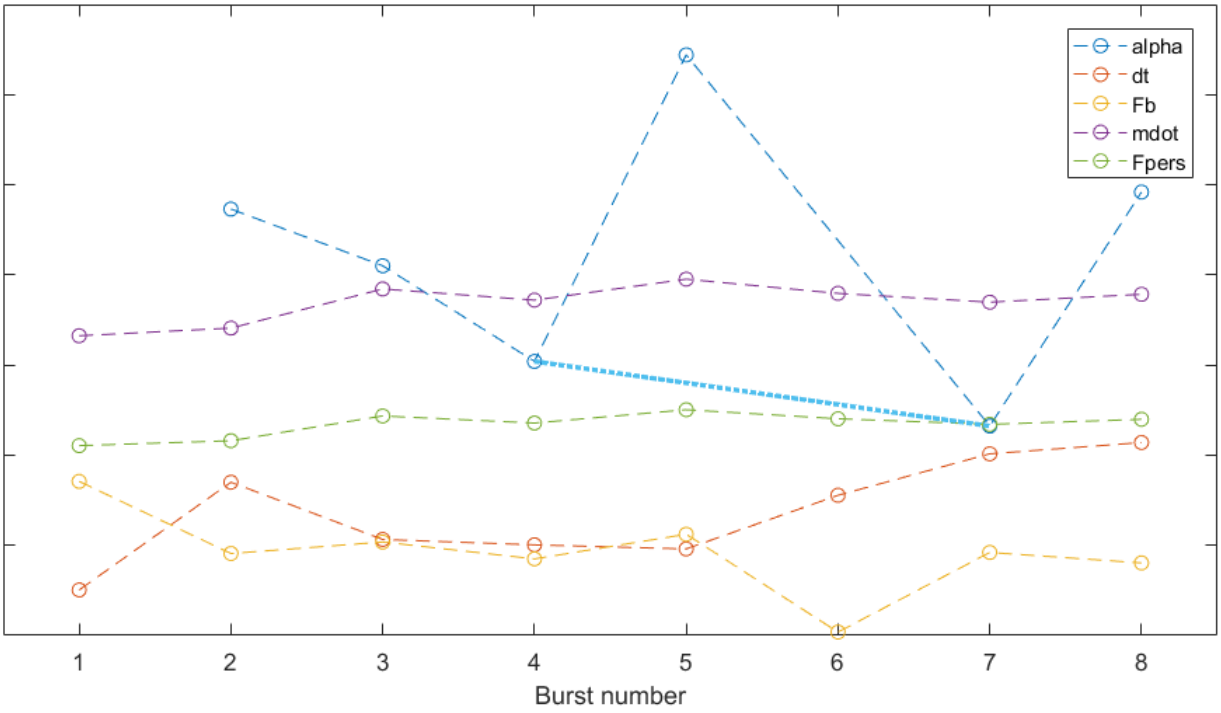

Figure 22: Graphic visualization of possible correlations between α, Δt, $F_{\mathrm{b,peak}}$, $\dot{m}$ and F_{pers}. All parameters has been multiplied by factors to clearly see all variations within the same plot. The cyan dotted line is the linear interpolation of α between 4 and 7, under the assumption that α for burst 5 is incorrect and neglected.

5.2 INTEGRAL

A search of SAX's coordinates in the INTEGRAL data archive revealed that the source had been observed in 7 revolutions within the same month NuSTAR had observed SAX. The revolutions used in this study is 1509, 1510, 1511, 1512, 1513, 1517 and 1521, spanning from February 18 2015 at 04:01:33 to March 24 2015 at 06:48:34. In the revolutions between, INTEGRAL has pointed elsewhere. In Appendix B all the science windows is listed.

During most of the observation, INTEGRAL has pointed towards the galactic center. This unfortunately mean that SAX is often located in the outer $3.5-4°$ of the center of the FOV making the data ill-defined. This means that it will be very difficult to spot bursts from the light curves. In Figure 23 the entire light curve for all revolutions shown. Revolution 1511 and 1512 is shown in $3-25$ keV, while the remaining has been shown in $3-10$ keV. The majority of X-ray photons emitted during a burst lies in the $3-10$ keV energy band, and as the data was already available in the $3-10$ keV energy band, this was chosen instead of re-running the data in $3-25$ keV. The most relevant data is in revolution 1511 and 1512, which is in the right energy band.

The time stamp of revolution 1512 is seen to match the data from NuSTAR. In this revolution the off-axis angle is mostly $> 4°$ (see Appendix B), making the data very ill-defined. In Figure 24 the NuSTAR and JEMX light curve is shown. The time stamp of both instruments has been converted to MJD to show them on same axis. The JEMX data is in TT, so an additional 66.184 s[17] has been subtracted to account for leap seconds Here it seen that JEMX unfortunately covers the data gaps of NuSTAR very poorly. In fact, the science windows of JEMX is not able to bridge a single data gap of NuSTAR. The data gap between burst 4 and 5 would have been nice to have covered, because of the suspected burst that lies within.

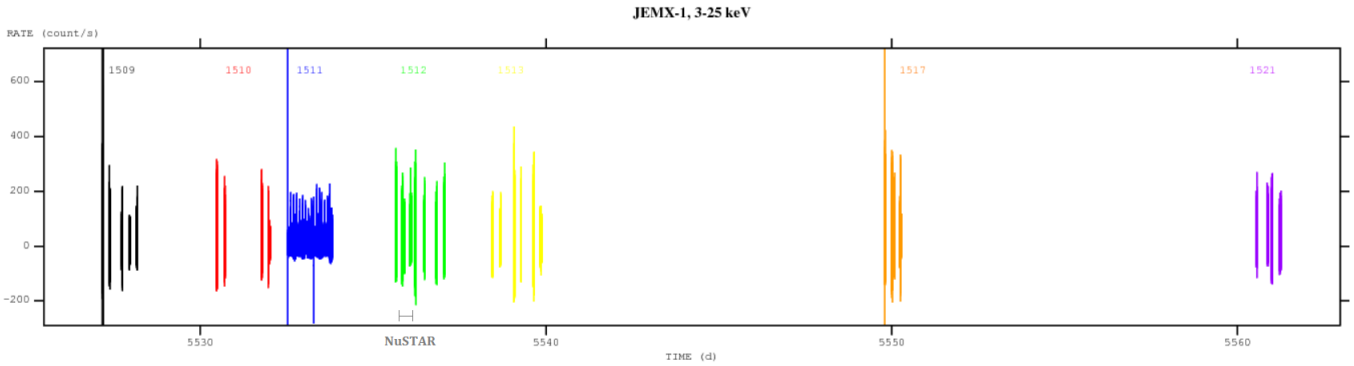

Figure 23: The entire JEMX-1 lightcurve for all revolutions in within the same time scale of NuSTAR's. The x-axis is shown in IJD.

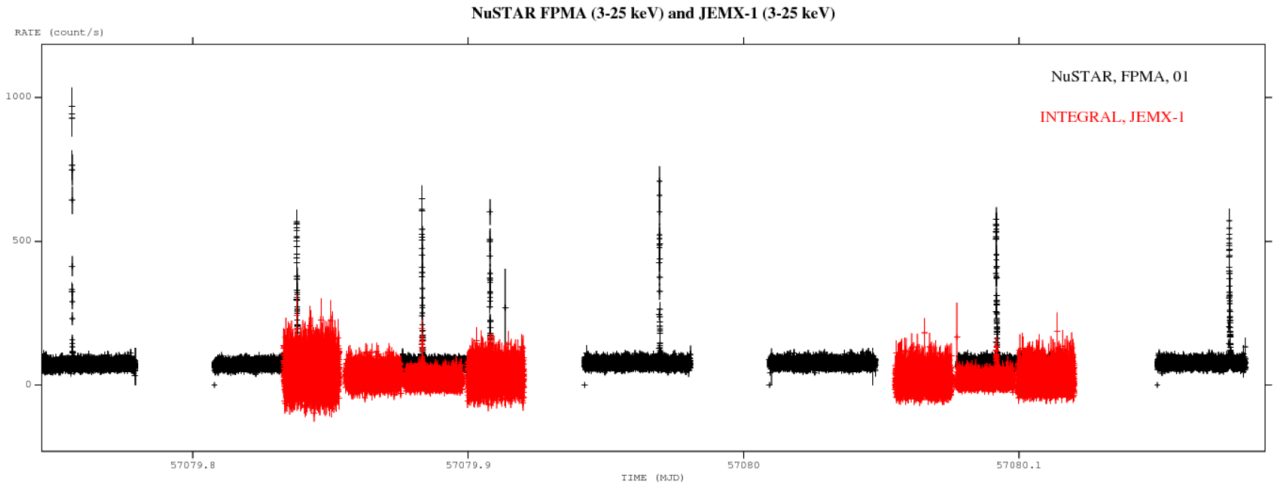

Figure 24: The entire NuSTAR light curve is shown along with the relevant science windows of 1512.

[17] Found by using NASA's HEASARC data/time converter by converting from UTC to TT, `https://heasarc.gsfc.nasa.gov/cgi-bin/Tools/xTime/xTime.pl`.

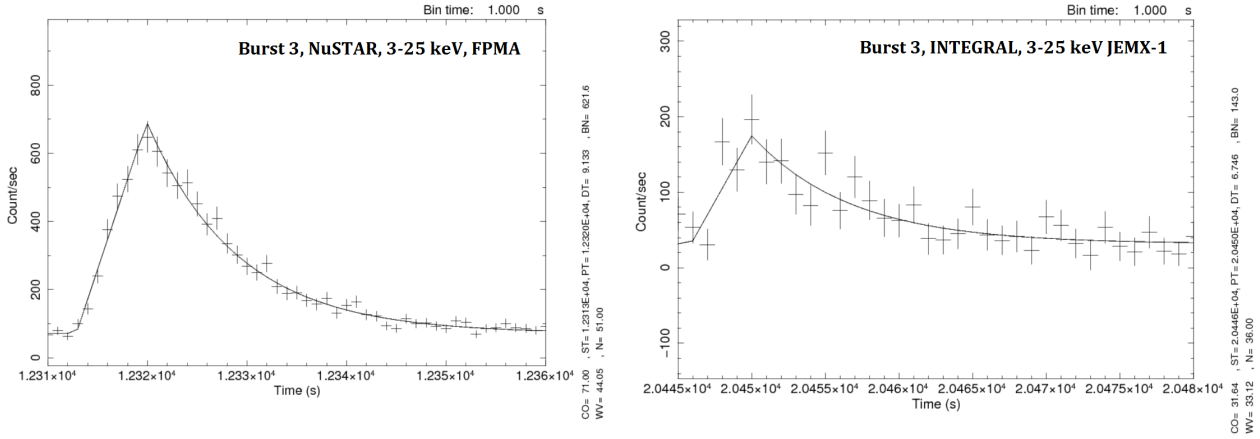

Figure 25: Fits of an exponential decay of burst 3 using `lcurve` on both NuSTAR and JEMX data points.

The error margins of the JEMX-1 data are very large, making it almost impossible to detect bursts. However, at least two burst can actually be seen by both instruments; burst 3 and 7. In the corresponding science windows SAX was within 1.4° and 2.3° respectively. Burst 2 show the difficulty of detecting bursts with JEMX-1 data. Bursts 2 would most likely have been interpreted as noise (and 4, for that matter) had one only looked at the JEMX-1 light curve. Data from JEMX-2 is likewise very ill-defined.

While it was possible to see bursts with JEMX-1, its still difficult to fit a proper model to the data points. In Figure 25 the fit of the models `CONS` and `BURS` is seen. The NuSTAR data points are much easier to find a fit for. The fit of NuSTAR data finds $\tau = 9.133$ s while the fit of JEMX-1 data finds $\tau = 6.746$ s. τ is expected to be within $10 - 15$ s for this type of burst[18], (Galloway et al., 2008). The figures use different time scales because of the different time zeroes.

NuSTAR and JEMX are two different instruments so the light curves cannot be directly compared. It is however possible to compare the two instruments by using the flux of the neutron star in the center of the Crab Nebula. This neutron star is extremely persistent in its X-ray emissions, and can be used for calibrating JEMX, but also used as a unit. By measuring the Crab with NuSTAR and INTEGRAL at a time near the observations, the average count count rate can be found which will equal 1 Crab. For NuSTAR, 1 Crab $\approx 612 \pm 25$ c/s, while for JEMX 1 Crab $\approx 124.31 \pm 0.41$ c/s. The Crab has well known flux at 1 Crab, so the peak of a burst can be expressed in terms of Crab to find the peak flux.

Burst 3 measured by NuSTAR had a peak count rate of ~ 650 c/s, which translates into 1.062 ± 0.041 Crab, which gives a peak flux of[19]: $F_{\mathrm{p,Crab}} = 27.263 \pm 1.049 \times 10^{-9}$ ergs cm^{-2} s^{-1}. This is a larger flux than the one found by `XSPEC`, which is because that `XSPEC` calculates an average flux across the whole time interval that is larger than the bin time. The flux calculated from the Crab is providing the most correct flux and the ratio of the two fluxes, 1.31, can be used to scale the unabsorbed flux. The ratio of the peak count rate and the spectral data counts should be close to this ratio. The count rate ratio was found by averaging the spectral data counts and peak count rate of FPMA and FPMB. This yielded the ratio of 2.03. A difference within $10 - 20\%$ would have been accepted. All fluxes and count rates has been found in the $3 - 25$ keV energy band. The cause of this discrepancy might be found in the short duration of persistent data before the burst, which `XSPEC` has used to determine the flux. Another explanation may be found in the model used. If the model has been too simple, and/or other phenomena has occurred during the burst that was not accounted for in the model, the flux may have been calculated incorrectly, yielding a wrong ratio.

The others bursts appeared to have approximately the same discrepancies in the ratio as burst 3. This suggest that a systematic error has occurred. The remaining burst light curves was in $3 - 42$ keV, but this should not be enough to give so large errors, as $\sim 90\%$ of the flux is expected to be in the range $3 - 25$ keV, Chenevez (a).

[18] Duration 10-100 seconds, not a helium flash.
[19] Converted using: `http://www.dsf.unica.it/~riggio/calcs.html`.

Burst 3 measured by JEMX-1 had a peak count rate of ~ 200 c/s, which translates into 1.611 ± 0.411 Crab, which gives a peak flux gives a peak flux of: $F_{\mathrm{p,Crab}} = 41.358 \pm 10.56 \times 10^{-9}$ ergs cm^{-2} s^{-1}. This is a larger flux than what would be expected of a burst like burst 3. The cause of this could be a vignetting correction that was too great, making the c/s in the light curve larger than the reality. The off-axis angle of burst 3 was 1.4, so the entire error might not be attributed to vignetting effects alone. The degrading of the instrument could also be a factor.

Since both the instruments was observing the same burst, NuSTAR could be used to calibrate JEMX. The ratio, of which the flux calculated from the peak of NuSTAR is greater than the flux calculated from the peak of JEMX, can be applied to the count rate of the peak measured by JEMX. This will yield the count rate that JEMX should have observed, to get a flux that corresponds to that of NuSTAR. The ratio of the newly found peak count rate and the originally measured count rate gives the factor that should be applied to the count rate of the JEMX light curve. This of course requires the NuSTAR data to be correct.

5.2.1 Revolution 1511

The 23$^{\mathrm{rd}}$ of February SAX started bursting regularly, making it a Target of Opportunity. During revolution 1511 it was directly observed using the Hexagonal dither which makes the data from revolution 1511 suitable for detecting bursts. In Figure 26 the light curve of revolution 1511 is plotted. As it is seen, at least 15 bursts can be identified.

The bursts observed in revolution 1511 has much more regular burst recurrence times when compared to the burst during the NuSTAR observation. The recurrence times is seen in Table 6. From the table it is seen to fall steadily from 130 minutes stabilizing around 111 minutes.

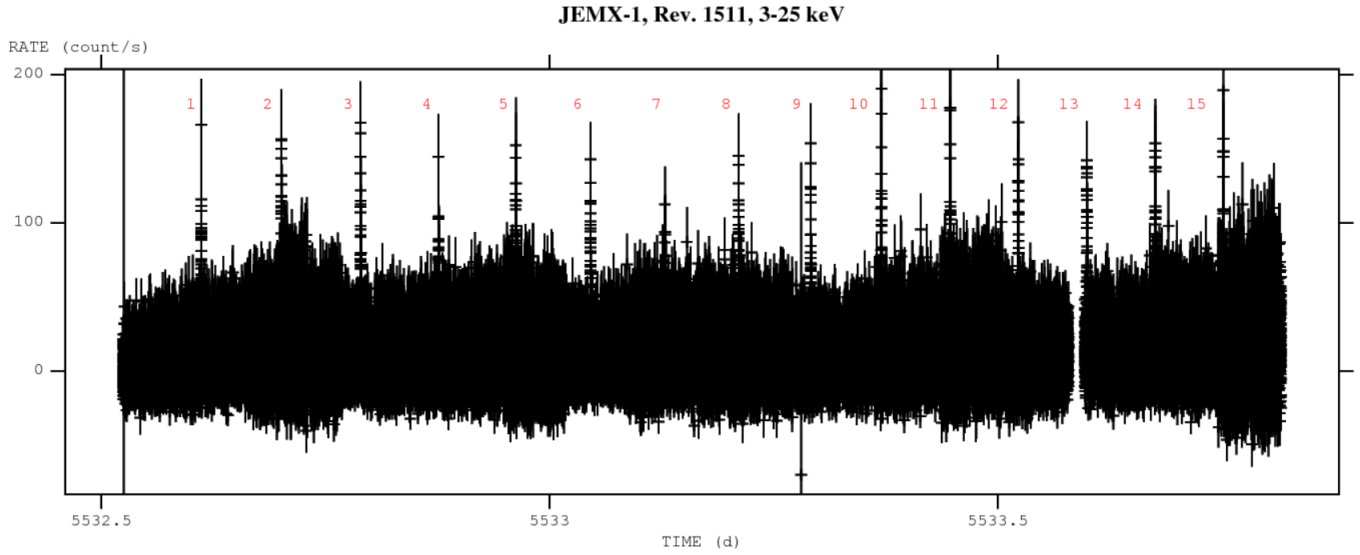

Figure 26: Light curve of revolution 1511 with the bursts marked. Time is in IJD.

A spectral analysis of each science window when expressed in c/s can be seen in Figure 27. These are the averaged fluxes of all science windows. The top panel shows all the science windows and the bottom shows all the science windows without bursts. This was done to reduce the increased count rate a burst would contribute to the average c/s of a science window. As it is seen, some spikes in the count rate is removed this way, but some unusual high and low c/s are still present. It is also seen that there is no apparent correlation between the two instruments, so they are not just 'out of sync'. From the data available, it would not be possible to determine which detector yields the correct flux, if any of them even does. It is chosen not to go in depth with each burst due to the inconsistency of the instruments, but short approximated characteristics will be given.

The average flux of each instrument is seen to be fairly equal, arriving at a value of ~ 8.6 c/s ≈ 69.28 mCrab $\approx 1.78 \times 10^{-9}$ ergs cm^{-2} s^{-1}. This is approximately half of the fluxes found in Table 4. It is however not an unlikely persistent flux.

Burst	**1-2**	**2-3**	**3-4**	**4-5**	**5-6**	**6-7**	**7-8**
$t_{\mathbf{rec}}$ **(min)**	130	131	128	125	122	121	120
Burst	**8-9**	**9-10**	**10-11**	**11-12**	**12-13**	**13-14**	**14-15**
$t_{\mathbf{rec}}$ **(min)**	116	114	111	111	111	112	110

Table 6: Recurrence times of the bursts detected in revolution 1511.

The persistent flux infers an average accretion of $\dot{m}_{\rm avg} \approx 6000$ g cm^{-2} s^{-1}. The bursts are thus expected to be triggered by thermally unstable He ignition in a mixed H/He environment. The rapid proton process slows the burst down, causing them to last > 10 s. This is approximately what the light curves show. All burst last $\sim 30 - 80$ s. No burst appeared to last < 10 s and have very steep rise, signifying that no helium flashes occurred, and thus the chances to see photospheric radius expansion in the spectral analysis would not be high.

Estimating the exponential decay time of the bursts to $\tau = 10$, yields an $\alpha \approx 55$ and a hydrogen to helium ratio of 50%. Between the highest and lowest peaks in the bursts, the α varied between $\sim 20 - 50$. The H/He ratio did get over 1 for the burst with the highest peak, even when fitting with an exponential decay model to find $\tau \approx 20$ and using the correct burst duration, persistent flux and recurrence time. A correction similar to that described previously to JEMX might solve this.

The persistent flux and accretion rate is shown in Figure 28.

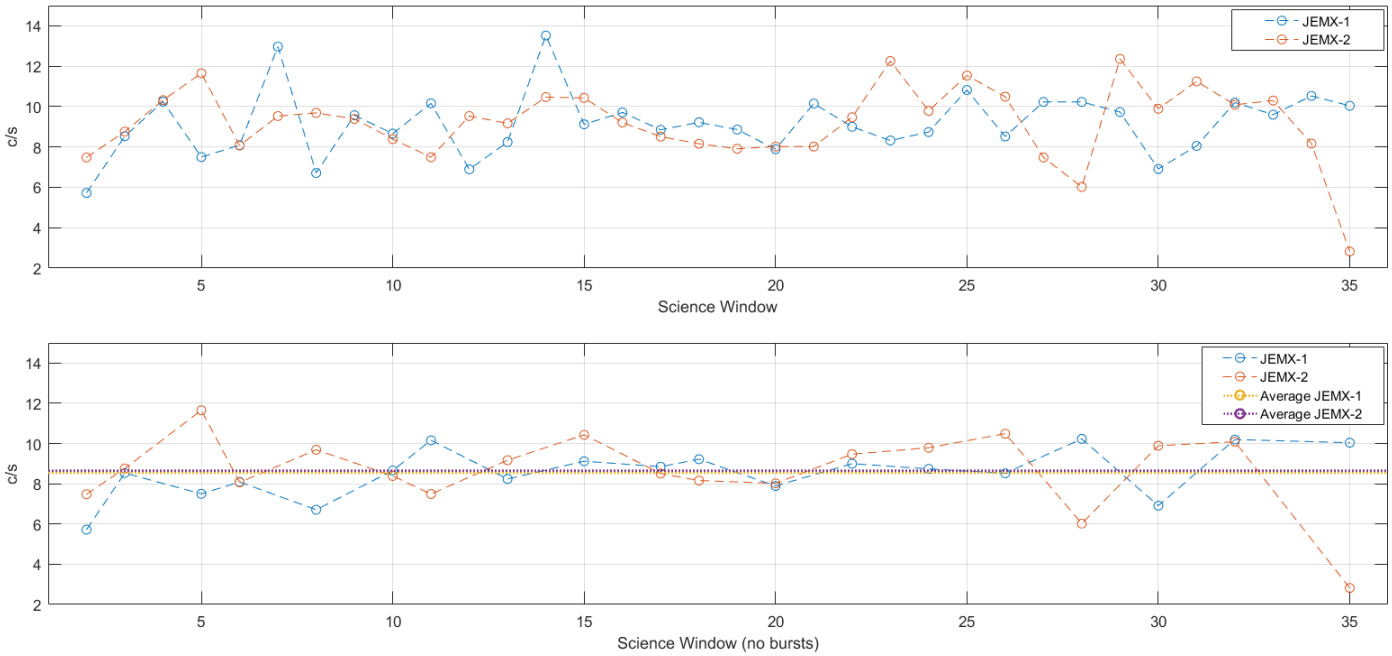

Figure 27: Plot of the intensity of each science window during revolution 1511. Top panel shows all science windows, including those with bursts in them. The bottom panel shows the intensity of the science windows that did not contain bursts.

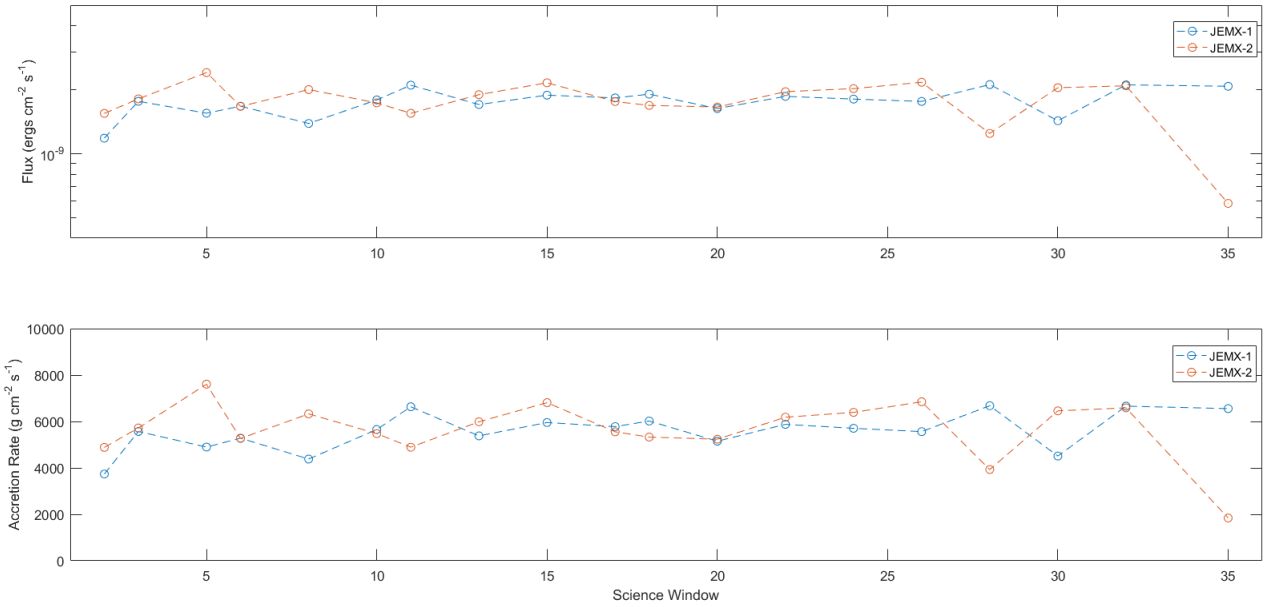

Figure 28: Top plot: The persistent flux in a logarithmic plot. Bottom plot: The accretion rate. Both plots uses the science windows without bursts.

6 Discussion

The light curves of the NuSTAR observation was plotted in the energy band $3 - 42$ keV. Throughout the study, the energy band used during calculations is $3 - 25$ keV. This introduced an error when doing calculations, but since 90% of the counts are expected to be within $3 - 25$ keV, the error was deemed so minor that the time resolved spectral analysis did not have to be redone. The maximum peak emission can through Wien's Displacement law be found to be within $5 - 6$ keV, so the most important part of the burst was caught in the $3 - 42$ keV energy band.

The systematic error of processing $3 - 42$ keV data as $3 - 25$ keV has not been included in the calculations. The errors from the instruments has been included, and has been overestimated to compensate for this. Another reason for the overestimation of errors is due to the nature of astrophysics in which even a precise measurement may be subject to objectively large errors. The method of application of error is seen in appendix C.

There was assigned no errors to the radius of the NS. There was found no external sources that had measured this, so a common NS radius was chosen. Almost all errors on parameters throughout the study, if not all, had asymmetric error margins. In all cases, the margins was averaged so a symmetric error could be applied during calculations. In most cases the relative difference between the upper and lower error margin was $\lesssim 0.5\%$. The radius determined by `XSPEC` did have much larger error margins, but these parameters was not used in any further calculations.

The large error on the radius during a burst is thought to arise due to the often large difference between the chosen counts per interval and the spectral data counts used by `XSPEC`. To improve the amount of spectral data counts, both FPMA and FPMB was used, which effectively doubled the amount of counts available. Still it was not enough to produce a χ_{R} that was satisfying in all cases. One could increase the temporal size of the intervals, but while this gives more well defined data, it come at the expense of the possibility to miss important variations in the spectral analysis.

When a burst peaks, the dead time becomes longer, and the software have to compensate for the lost photons by estimating how many photons have hit the detector during the dead time. The longer the dead time, the fewer spectral data counts does `XPSEC` have to perform analysis on. This may prove a problem for very energetic bursts. Here it is also difficult to get the right amount of counts per interval. In this study it was chosen to be more important getting the right amount of counts per interval than staying within the thresholds normally used when performing time resolved spectral analysis. Whether this method could introduce some problems is unknown. Perhaps by strictly using the 25%, 90% and 25% thresholds you actually accounts for the longer dead time during the peak of a burst. One could expect that the duration of a peak interval should be a factor shorter than a given decay interval equal the ratio of the two intervals flux. While it is seen that decay intervals are shorter than peak intervals, this ratio is not seen.

When working with the RATE_ORIG data, the spectral data counts were $99 - 100\%$ of the counts per interval chosen. This data set uses only the counts detected by the detector, and is thus not corrected for dead time. This was thought to improve the χ statistic, but it was found that the method had little to no impact on the determination of the radius.

The 06 data type was so ill defined that it could only be of little use. The light curve from the 06 data was however extremely valuable, as it revealed a burst happening moments after the 01 data stream ended. The need for a complete light curve as possible became very apparent when burst 5 showed a H/He ratio that did not make sense. It suggest a burst might be missing between burst 4 and 5. Also between burst 1 and 2 and 7 and 8 could bursts be hiding. It would make sense compared the recurrence times, and, in the case of burst 5, the H/He ratio.

The recurrence times of the NuSTAR observation are more sporadic those in revolution 1511 observed by JEMX. The recurrence times in 1511 were very stable and the time fell steadily stabilizing around 111 minutes. The average of recurrence times in 1511 is ≈ 1.5 times longer than that observed by NuSTAR. This figure is even higher if bursts are hidden in the data gaps of the NuSTAR observation. No bursts are expected to be hiding in data gaps of 1511. The recurrence time of 1511 did not appear to follow

any trend in the accretion rate. The accretion rate, while poorly defined, averaged around $\approx$ 6000 g cm^{-2} s^{-1}, which suggest that hydrogen should burn stably into helium, which should ignite when the temperature becomes sufficiently high. It is however not the characteristic light curves of pure helium bursts that are seen. The average persistent flux is a factor of $\approx 2-3$ times lower than the one detected a few days later in the NuSTAR observation. If the flux is a factor $2-3$ higher, so is the accretion rate, and thus a mixed H/He ignition is expected. If the temperature of the layers increases slowly over the course of the observation, helium might ignite faster causing the fall in recurrence time. When the recurrence time falls and the accretion rate stays constant, the peak flux is expected to fall throughout the observation. The peak fluxes is however seen to rise and fall at random.

The accretion rate during the NuSTAR observation appeared rather constant. The recurrence times, peak flux and fluence of the burst did however not. Like Galloway et al. (2008) summarised for previous bursts of SAX, the long and short bursts appeared to alternate independently of the persistent flux. Burst 4 had a persistent flux similar to that of Burst 7 and 8, but the burst duration of the latter two was twice as long as burst 4. The α appeared to take a dip and then rise again over the course of the observation if the α of burst 5 is neglected.

Of all burst observed by NuSTAR, burst 1 was the only one that exhibited clear indications of photospheric radius expansion. From this a local Eddington luminosity limit could be determined which was $\approx 10-30\%$ lower than the expected L_{Edd} for LMXB in globular clusters, (Kuulkers et al., 2003), depending on the study. The composition of the photosphere impacts the flux required to reach PRE suggesting that the photosphere contains more helium than hydrogen due to the lower L_{Edd} calculated, (Galloway et al., 2008). Burst 2 and 8 exhibited signs of PRE (dip in color temperature and nearly constant flux), but the peak flux did not reach high enough levels to be a PRE.

The reason of the bulge observed seconds after the peak of the bursts is still not well understood. It may indicate that the spin of the NS has an impact on the spread of the explosion through the Coriolis effect. Another explanation might be that the spread of the explosion 'collides' on the opposite side of the NS resulting in a flare. Simulations of this effect has however shown not to match what is seen, (Chenevez, a). The accreted matter on the NS cannot be assumed to be evenly distributed, as illustrated in Figure 3. This may also affect the spread the burst. From this one thing is clear: Isotropy of the the burst cannot be assumed, and perhaps the ξ_{b} and ξ_{p} should be altered.

The accretion disc will during a burst be dilated due radiation pressure of the thermonuclear explosion. The accretion disc reflects some of the photons coming from the burst which will result in a higher flux than the burst actually released per square centimetre. This effect is not accounted for in the models used to extract a flux from the burst. In general the model `TBabs(bbodyrad)` gives a fine estimate of the various parameters, but it does not account for phenomena such as the accretion disc dilation and unevenly distributed matter, and thus gives wrong estimates of the reality. It also assumes that the decay of the burst can be modelled with an exponential decay, but recent studies suggest that the decay is more suitable to be fitted with a power law, (Chenevez, a). Its possible to improve the results by adding additional models and components, but its beyond the scope of this study to experiment with combinations of the myriad of models included in `XSPEC`.

The model to describe the persistent was improved, since `bbodyrad` and `bkn2po` could not be extrapolated outside the energy band chosen, and there could thus not be extracted a persistent flux which made sense. The combination of `diskbb` and `compTT` yielded more reliable results, but the models might be extended further to give even more precise estimates.

Using `lcurve` to fit an exponential decay to the bursts in the NuSTAR observation proved to be easier than in the JEMX observation. The light curves was much more well-defined in the NuSTAR observation, and through trial and error a probable modelled could be fitted with the light curve. Due to the large errors margins of the light curve from the JEMX data, it was difficult to fit the model. The peak count rate often had to be assumed, since the count rate behaved strange during peaks (moving up and down at apparently random). The found τ for the burst of the NuSTAR observation yielded α similar to the α found through the time resolved spectral analysis. The τ required to match the accretion rate and burst duration and peak flux for the 1511 data was a about twice the τ found using `lcurve`.

The measured average intensity of the science windows in revolution 1511 revealed that JEMX-1 and JEMX-2 yielded remarkably different results, which was not correlated in any way. The instrument has degraded over the years, and has surpassed its expected operational lifetime, (Kuulkers, 2015), so the data demands quite comprehensive processing to produce precise scientific data.

It was attempted to compare the two instruments by converting the peak of bursts into units of Crab. This proved to provide even better estimates of the peak fluxes than those obtained through determination of τ and by using `XSPEC`. After the conversion it should have been possible to compare the two instruments, and even calibrate JEMX using NuSTAR, but the ratios of the peak flux measured by `XSPEC` and then flux measured from the peak did not match the ratio of peak count rate versus the spectral data counts, which suggest a systematic error have sneaked in the calculations or conversions somewhere. Perhaps the short duration persistent flux observed prior to burst 3 and 7 could have influenced the results. It did though become clear that JEMX overestimated the peak fluxes, which was found to be $\approx 41\times10^{-9}$ ergs cm^{-2} s^{-1}, which is approximately twice as large as expected for burst not exhibiting PRE.

The comparison was also complicated since many data points in the JEMX light curve revealed negative count rate. It was meant to scale the NuSTAR and JEMX light curve that was in common, by finding the ratio of which the NuSTAR was greater than JEMX, and then apply that factor to JEMX, but this would make negative data point even more negative. It could have been done the other way around however.

The NuSTAR observation was rerun with `run_nuproducts` using the energy bands $3-10$ keV and $10-25$ keV. This allowed to find the ratio of the soft and hard X-rays. The ratio of the average intensity over the entire observation was found to 0.125, which suggest that the accretion disc is well developed, (Chenevez, b). A color-color diagram of the ratio of soft colors versus the ratio of hard colors using the energy bands $3-10$ keV, $6-10$ keV, $10-20$ keV and $20-60$ keV is seen in Figure 29. The overall trend has been drawn in grey. The diagram has been made by finding the average intensity of the entire persistent before the bursts. The observation started with a burst exhibiting PRE, and from that the line between the dots can be tracked to see the evolution throughout the observation, which resembles the "atoll" shape.

Ideally the persistent should be divided into a lot of intervals of e.g. 20 seconds duration, and then plot all of those to be able to see a much clear shape and more detail.

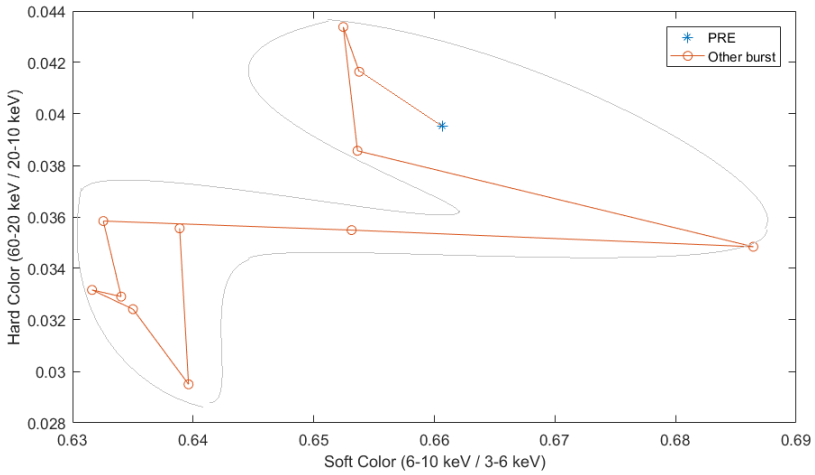

Figure 29: Color-color plot. The soft colors has been plotted against the hard colors. The trend in the movement of the state is shown in grey.

7 Conclusion

The behaviour of low-mass X-ray binaries was accounted for, and a short characteristic was given of NuSTAR and JEMX. The pipeline of each instrument for the production of scientific data was described. The source chosen for this study was the LMXB SAX J174853-202202 which was observed in outburst by NuSTAR. To aid in the study, data from JEMX used as well. This enabled comparison of the two instruments and to rule out extreme data.

The NuSTAR observation was successfully processed using the available software. From the light curves 8 distinct bursts could be identified with recurrence time varying between $36 - 117$ minutes. The 06 data type revealed that a burst was nearly missed in a data gap. Non-sensible parameters suggested that at least one burst was lost in the data gaps. A time resolved spectral analysis was performed through which the persistent flux was determined to be within $\approx 4.2 - 5 \times 10^{-9}$ ergs cm^{-2} s^{-1} which was in agreement with expected values.

The bursts was modelled using a black body radiation model, and yielded well defined fluxes and color temperatures. The radius inferred from the spectral analysis was very ill-defined which were attributed to the relatively small amounts of spectral data counts in each burst interval. The bolometric flux ranged between $16 - 22.5 \times 10^{-9}$ ergs cm^{-2} s^{-1} for non photospheric radius expansion bursts. One burst exhibited clear indications of PRE and reached a peak bolometric flux of 34×10^{-9} ergs cm^{-2} s^{-1}. All the found fluxes was in agreement with previous studies of SAX 174853-202202.

There was found no correlation of the persistent flux and the burst duration. The accretion rate was found fairly constant at 0.2 of $\dot{m}_{\mathrm{Edd}}$. This suggested that the bursts occurred when helium starts to burn steadily and ignites when temperatures got sufficiently high. The PRE burst had $\dot{m} \approx 0.2\,\dot{m}_{\mathrm{Edd}}$ which was contradicting the theory, as the expected accretion rate was thought to be below $0.1\,\dot{m}_{\mathrm{Edd}}$.

JEMX observed the source in the same time frame as the NuSTAR data, but it turned out that off-axis angle was very high rendering the data very ill-defined. It was possible to see at least 2 burst that JEMX and NuSTAR had in common. No additional bursts in NuSTAR time frame was detected with JEMX.

SAX 174853-202202 was a Target of Opportunity a few days prior to the NuSTAR observation during revolution 1511, in which the data was more well-defined. The average flux readings of each science window showed that there was large, uncorrelated discrepancies between JEMX-1 and JEMX-2 readings. The persistent flux and accretion rate was determined, and showed a flux half of that measured by the `XSPEC` during the NuSTAR observation. The accretion rate was approximately one third of that of the NuSTAR observation.

A comparison of NuSTAR and JEMX was attempted by converting the count rates into mCrab, but a systematic error caused the results to be non-comparable. The flux from the peak count rate during revolution 1511 was 41×10^{-9} ergs cm^{-2} s^{-1}, which was approximately twice as large as expected for the burst types. None of the burst during revolution 1511 exhibited the traits indicating a helium flash in which PRE is often seen.

Bibliography

Arnaud, K., Gordon, C., & Dorman, B. (2017). Xspec, an x-ray spectral fitting package. `https://heasarc.gsfc.nasa.gov/xanadu/xspec/manual/`.

Chenevez, J. Private communication.

Chenevez, J. X-ray binaries. Slides.

Chenevez, J. (2010). Puzzling thermonuclear burst behaviour from the transient low-mass x-ray binary igr j17473-2721. *Proceedings of Science*.

Chernyakova, M., Kretschmar, P., Neronov, A., Beckmann, V., & Pavan, L. (2015). *JEM-X Analysis User Manual*. California Institute of Technology and ASI Science Data Center.

Condon, J. J. & Ransom, S. M. (2016). Essential radio astronomy, chapter 6 - pulsars. `http://www.cv.nrao.edu/~sransom/web/Ch6.html`.

Cotter, G. (2012). High-energy astrophysics. `http://www-astro.physics.ox.ac.uk/~garret/teaching/lecture7-2012.pdf`.

Formulas, A. (2012). Temperature in kev to kelvin conversion. `http://astrophysicsformulas.com/astronomy-formulas-astrophysics-formulas/temperature-in-kev-to-kelvin-conversion/`.

Forster, K., Grefenstette, B., & Madsen, K. (2014). *NuSTAR DATA ANALYSIS Quickstart Guide*. California Institute of Technology.

Freedmann, R. A. & Kaufmann, W. J. (2008). *Universe*. W.H. Freedmann Company.

Galloway, D. K., Muno, M. P., Hartman, J. M., Psaltis, D., & Chakrabarty, D. (2008). Thermonuclear (type i) x-ray bursts observed by the rossi x-ray timing explore. *The Astrophysical Journal Supplement Series*.

Harrison, F. A., Craig, W. W., Christensen, F. E., Hailey, C. J., Zhang, W. W., Boggs, S. E., Stern, D., Cook, W. R., Forster, K., Giommi, P., Grefenstette, B. W., Kim, Y., Kitaguchi, T., Koglin, J. E., Madsen, K. K., Mao, P. H., Miyasaka, H., Mori, K., Perri, M., Pivovaroff, M. J., Puccetti, S., Rana, V. R., Westergaard, N. J. S., Willis, J., Zoglauer, A., An, H., Bachetti, M., Barrie're, N. M., Bellm, E. C., Bhalerao, V., Brejnholt, N., Fuerst, F., Liebe, C. C., Markwardt, C. B., Nynka, M., Vogel, J. K., Walton, D. J., Wik, D. R., Alexander, D. M., Cominsky, L. R., Hornschemeier, A. E., Hornstrup, A., Kaspi, V. M., Madejski, G. M., Matt, G., Molendi, S., Smith, D. M., Tomsick, J. A., Ajello, M., Ballantyne, D. R., Balokovic, M., Barret, D., Bauer, F. E., Blandford, R. D., Brandt, W. N., Brenneman, L. W., Chiang, J., Chakrabarty, D., Chenevez, J., Comastri, A., Dufour, F., Elvis, M., Fabian, A. C., Farrah, D., Fryer, C. L., Gotthelf, E. V., Grindlay, J. E., Helfand, D. J., Krivonos, R., Meier, D. L., Miller, J. M., Natalucci, L., Ogle, P., Ofek, E. O., Ptak, A., Reynolds, S. P., Rigby, J. R., Tagliaferri, G., Thorsett, S. E., Treister, E., & Urry, C. M. (2013). The nuclear spectroscopic telescope array (nustar) high-energy x-ray mission. *Astrophysical Journal*, 770(2), 103.

Kuulkers, E. (2015). *Announcement of Opportunity for Observing Proposals (AO-13)*. INTEGRAL Science Operations Centre.

Kuulkers, E., den Hartog, P., in't Zand, J., Verbunt, F., Harris, W., & Cocchi, M. (2003). Photospheric radius expansion x-ray bursts as standard candles. *Astronomy and Astrophysics*, 399(2), 663–680.

MIPT (2016). X-ray pulsars fade as propeller effect sets in. `https://mipt.ru/english/news/x_ray_pulsars_fade_as_propeller_effect_sets_in`.

Perri, M., Puccetti, S., Spagnuolo, N., Ficcadenti, R., Davis, A., Forster, K., Grefenstette, B., Harrison, F., & Madsen, K. (2016). *The NuSTAR Data Analysis Software Guide*. California Institute of Technology and ASI Science Data Center.

Seward, F. D. & Charles, P. A. (2010). *Exploring the X-ray Universe*, chapter 11. Cambridge University Press.

Singh, K. P. (2005). Techniques in x-ray astronomy. *Resonance*.

Appendix

A NuSTARDAS pipeline

The NuSTARDAS pipeline to process Level 1 event files into Level 3 Scientific data products.

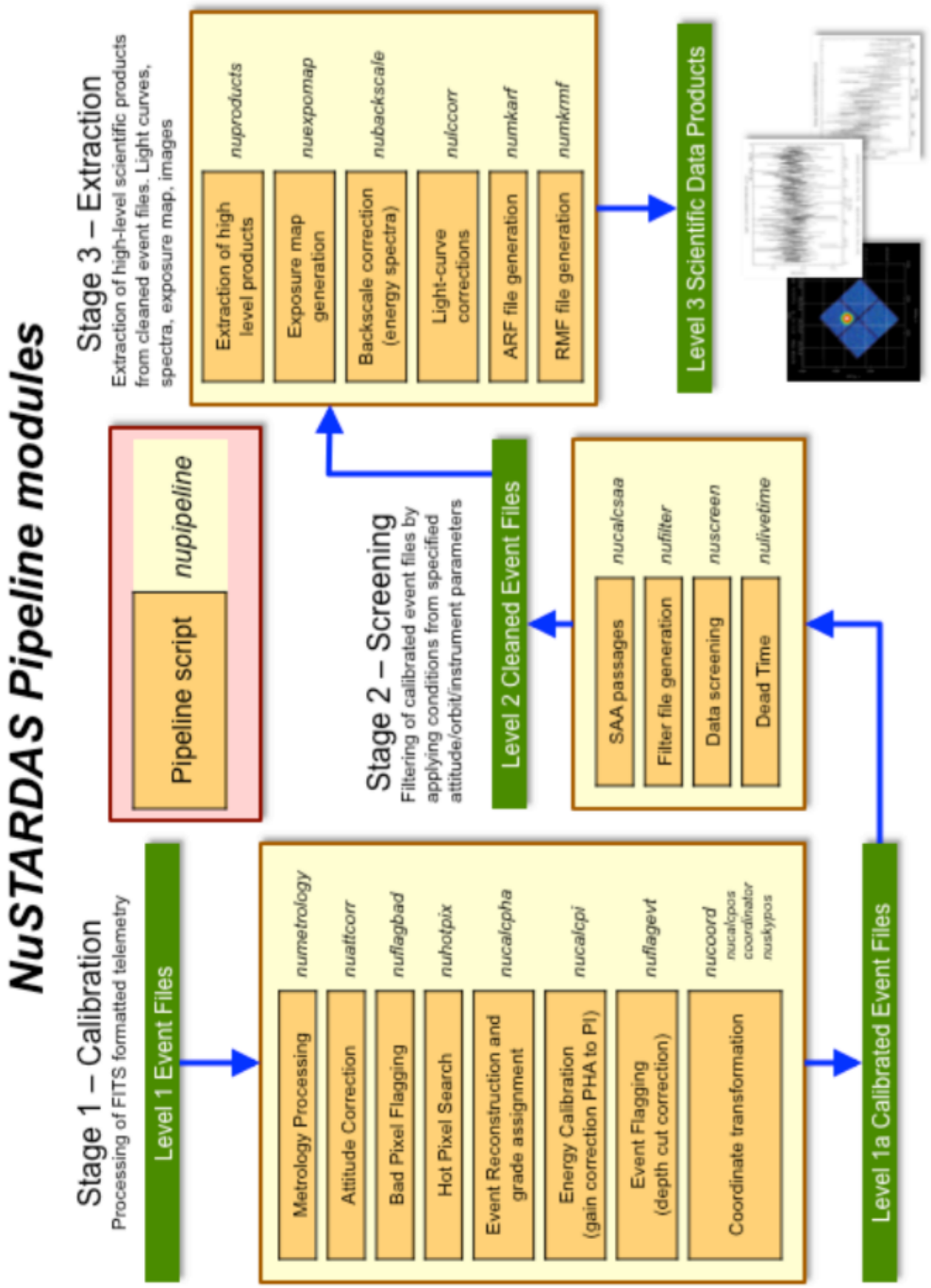

B Science windows

The list is generated by finding in which revolution SAX's coordinates came within the FOV of INTEGRAL. `ra0` and `dec0` is SAX's coordinates, `radius` is the radius of the field of view. The first column is the name of the revolution and science window number. The second and third column is the on-axis coordinates. Column 5 is the time stamp, and column 6 is the time stamp in IJD. Column 7 is the length of the science window and column 8 and 9 describes whether JEMX-1 and 2 is in the FULL mode or anything else. The tenth column is the off-axis angle in degrees.

```
// Results from find_swid_radec
// created 2017-03-03T12:03:37
// ra0  = 267.220; deg
// dec0 = -20.360; deg
// lon0 =   7.729; deg
// lat0 =   3.801; deg
// radius =   5.000; deg
// rev_begin = 1502
// rev_end   = 1524
150900010010 269.4850 -24.2691 -89.635 2015-02-18T03:50:18 5527.161 593  * * 4.43 67
150900020010 269.4810 -24.4632 -89.530 2015-02-18T04:01:36 5527.168 1802 * * 4.60 143
150900110010 267.1683 -24.9315 -90.248 2015-02-18T08:50:17 5527.369 1790 F F 4.57 153
150900270010 270.7984 -22.2231 -90.377 2015-02-18T17:28:47 5527.729 592  F F 3.82 140
150900280010 270.7975 -22.6449 -90.119 2015-02-18T17:40:09 5527.737 1802 F F 4.04 347
150900370010 268.5121 -23.0853 -90.744 2015-02-18T22:29:27 5527.938 1790 F F 2.98 724
150900380010 266.2105 -23.6314 -91.364 2015-02-18T23:01:27 5527.960 1798 F F 3.40 574
150900470010 263.8719 -23.9920 -92.080 2015-02-19T03:50:01 5528.161 1801 F F 4.77 81
151000240010 269.5087 -24.3187 -89.697 2015-02-21T11:06:09 5530.463 593  F F 4.49 61
151000250010 269.5128 -24.4954 -89.619 2015-02-21T11:17:33 5530.471 2001 F F 4.65 141
151000340010 267.1954 -24.9949 -90.351 2015-02-21T16:36:04 5530.692 1991 F F 4.63 145
151000760010 272.1812 -20.4307 -90.694 2015-02-22T18:17:29 5531.763 593  F F 4.65 41
151000770010 272.1651 -20.5772 -90.622 2015-02-22T18:28:49 5531.771 1802 F F 4.64 131
151000850010 270.4062 -23.1678 -89.901 2015-02-22T23:11:01 5531.967 1789 F F 4.08 330
151000860010 269.8943 -21.0496 -91.140 2015-02-22T23:43:13 5531.989 1791 F F 2.59 862
151000870010 267.6186 -21.5093 -91.720 2015-02-23T00:15:01 5532.011 2274 F F 1.21 1725
151100010010 267.3795 -20.2915 -92.311 2015-02-23T12:09:33 5532.507 592  * * 0.16 573
151100020010 267.3643 -20.3502 -92.287 2015-02-23T12:20:53 5532.515 3002 * * 0.14 2921
151100030010 265.4636 -21.2726 -92.561 2015-02-23T13:13:00 5532.551 2990 F F 1.88 1867
151100040010 265.5759 -19.2603 -93.316 2015-02-23T14:04:45 5532.587 3001 F F 1.90 1862
151100050010 267.4534 -18.3454 -93.125 2015-02-23T14:56:42 5532.624 3001 F F 2.03 1785
151100060010 269.2431 -19.4140 -92.099 2015-02-23T15:48:47 5532.660 2988 F F 2.12 1718
151100070010 269.1782 -21.4201 -91.199 2015-02-23T16:40:50 5532.696 2993 F F 2.11 1727
151100080010 267.2756 -22.3512 -91.490 2015-02-23T17:32:36 5532.732 3000 F F 1.99 1805
151100090010 266.7294 -20.6507 -92.384 2015-02-23T18:24:32 5532.768 3000 F F 0.54 2674
151100100010 264.8235 -21.5756 -92.678 2015-02-23T19:16:42 5532.804 2989 F F 2.55 1467
151100110010 264.9427 -19.5655 -93.379 2015-02-23T20:08:23 5532.840 3001 F F 2.28 1631
151100120010 266.8241 -18.6539 -93.167 2015-02-23T21:00:21 5532.876 3001 F F 1.75 1953
151100130010 268.6156 -19.7248 -92.159 2015-02-23T21:52:28 5532.912 2989 F F 1.46 2118
151100140010 268.5502 -21.7293 -91.288 2015-02-23T22:44:31 5532.948 2995 F F 1.85 1888
151100150010 266.6388 -22.6596 -91.603 2015-02-23T23:36:32 5532.984 2989 F F 2.36 1577
151100160010 266.7661 -19.9784 -92.632 2015-02-24T00:28:28 5533.021 3001 F F 0.57 2658
151100170010 264.8599 -20.9036 -92.912 2015-02-24T01:20:26 5533.057 3001 F F 2.27 1636
151100180010 264.9863 -18.8927 -93.606 2015-02-24T02:12:23 5533.093 2999 F F 2.56 1461
151100190010 266.8681 -17.9885 -93.407 2015-02-24T03:04:17 5533.129 3001 F F 2.39 1564
151100200010 268.6479 -19.0696 -92.411 2015-02-24T03:56:12 5533.165 3000 F F 1.86 1882
151100210010 268.5679 -21.0726 -91.568 2015-02-24T04:48:26 5533.201 2994 F F 1.45 2127
151100220010 266.6625 -21.9942 -91.844 2015-02-24T05:40:25 5533.237 2989 F F 1.71 1964
151100230010 267.3880 -19.6728 -92.558 2015-02-24T06:32:42 5533.273 4464 F F 0.71 3834
151100240010 265.4951 -20.5972 -92.798 2015-02-24T07:49:13 5533.327 2990 F F 1.63 2013
151100250010 265.6167 -18.5888 -93.496 2015-02-24T08:40:57 5533.362 3002 F F 2.33 1604
151100260010 267.4885 -17.6805 -93.329 2015-02-24T09:32:55 5533.398 3001 F F 2.69 1386
151100270010 269.2689 -18.7573 -92.348 2015-02-24T10:25:03 5533.435 2989 F F 2.51 1489
151100280010 269.1945 -20.7608 -91.490 2015-02-24T11:17:01 5533.471 2994 F F 1.89 1861
151100290010 267.2960 -21.6874 -91.758 2015-02-24T12:09:03 5533.507 2989 F F 1.33 2194
151100300010 267.9952 -20.0265 -92.184 2015-02-24T13:00:53 5533.543 3104 F F 0.80 2607
151100310010 266.0977 -20.9622 -92.443 2015-02-24T14:18:09 5533.597 2992 F F 1.21 2268
151100320010 266.2066 -18.9533 -93.175 2015-02-24T15:09:59 5533.633 3000 F F 1.70 1980
151100330010 268.0743 -18.0378 -92.981 2015-02-24T16:01:53 5533.669 5013 F F 2.46 2548
151100330020 268.0743 -18.0378 -92.981 2015-02-24T17:25:23 5533.727 1478 F F 2.46 751
151100340010 269.8652 -19.1019 -91.969 2015-02-24T17:52:13 5533.746 2990 F F 2.79 1322
151100350010 269.8055 -21.1061 -91.095 2015-02-24T18:44:15 5533.782 2994 F F 2.53 1479
151200240010 272.3670 -20.7631 -90.258 2015-02-26T15:31:06 5535.647 594  F F 4.84 20
```

```
151200250010 272.3693 -20.7181 -90.261 2015-02-26T15:42:23 5535.655 1802 F F 4.84 59
151200330010 270.5990 -23.3069 -89.787 2015-02-26T19:58:47 5535.833 1792 F F 4.30 250
151200340010 270.0985 -21.1891 -90.845 2015-02-26T20:31:01 5535.855 1793 F F 2.82 783
151200350010 267.8231 -21.6446 -91.487 2015-02-26T21:03:03 5535.878 1799 F F 1.40 1294
151200360010 268.2872 -23.7762 -90.514 2015-02-26T21:35:19 5535.900 1794 F F 3.56 518
151200430010 265.9548 -24.1729 -91.324 2015-02-27T01:19:03 5536.056 1801 F F 3.99 364
151200440010 265.5366 -22.0401 -92.175 2015-02-27T01:51:16 5536.078 1795 F F 2.30 970
151200450010 263.2181 -22.4237 -92.905 2015-02-27T02:23:08 5536.100 1800 F F 4.26 267
151200500010 270.3335 -23.6953 -89.735 2015-02-27T05:06:18 5536.213 592  F F 4.41 70
151200510010 270.3389 -23.7382 -89.726 2015-02-27T05:17:38 5536.221 1915 F F 4.45 212
151200600010 268.0354 -24.2164 -90.471 2015-02-27T11:05:45 5536.463 1800 F F 3.93 385
151200610010 265.7004 -24.6787 -91.261 2015-02-27T11:37:57 5536.485 1798 F F 4.54 165
151200760010 269.4692 -23.7704 -90.041 2015-02-27T19:42:28 5536.822 592  F F 4.00 119
151200770010 269.4692 -23.7704 -90.041 2015-02-27T19:53:48 5536.830 1801 F F 4.00 361
151200860010 267.1506 -24.2423 -90.803 2015-02-28T00:41:45 5537.030 1801 F F 3.88 402
151200870010 264.8141 -24.6728 -91.620 2015-02-28T01:13:56 5537.052 1799 F F 4.85 53
151300240010 270.1103 -23.0620 -90.053 2015-03-01T10:39:51 5538.445 593  F F 3.81 141
151300250010 270.1103 -23.0620 -90.053 2015-03-01T10:51:12 5538.453 1807 F F 3.81 430
151300340010 267.8033 -23.5301 -90.805 2015-03-01T15:39:12 5538.653 1801 F F 3.22 643
151300350010 265.4791 -23.9579 -91.602 2015-03-01T16:11:27 5538.675 1800 F F 3.94 381
151300500010 270.1353 -24.2932 -89.615 2015-03-02T01:25:16 5539.060 592  F F 4.77 27
151300510010 270.1353 -24.2932 -89.615 2015-03-02T01:36:37 5539.068 1802 F F 4.77 83
151300600010 267.8093 -24.7743 -90.424 2015-03-02T06:24:36 5539.268 1796 F F 4.45 198
151300760010 271.2742 -22.6693 -89.725 2015-03-02T15:01:51 5539.627 593  F F 4.42 69
151300770010 271.2733 -22.7472 -89.698 2015-03-02T15:13:13 5539.635 1802 F F 4.46 194
151300860010 268.9761 -23.2178 -90.417 2015-03-02T20:02:05 5539.835 1795 F F 3.29 614
151300870010 266.6575 -23.6724 -91.202 2015-03-02T20:34:12 5539.858 1799 F F 3.35 593
151700570010 272.3478 -21.4588 -89.403 2015-03-12T18:56:08 5549.790 592  F F 4.91 10
151700580010 272.3470 -21.4007 -89.405 2015-03-12T19:07:28 5549.797 2002 F F 4.90 39
151700660010 270.5370 -23.9763 -89.689 2015-03-12T23:50:24 5549.994 2001 F F 4.74 102
151700670010 270.0670 -21.8525 -90.176 2015-03-13T00:25:42 5550.019 2000 F F 3.05 781
151700680010 267.7699 -22.2874 -90.976 2015-03-13T01:00:56 5550.043 2001 F F 1.99 1203
151700690010 268.2065 -24.4264 -90.574 2015-03-13T01:36:30 5550.068 1999 F F 4.17 333
151700760010 265.8620 -24.7949 -91.517 2015-03-13T05:43:36 5550.239 2001 F F 4.61 157
151700770010 265.4686 -22.6626 -91.817 2015-03-13T06:18:53 5550.264 2000 F F 2.82 872
152100640010 264.4578 -23.9792 -92.276 2015-03-23T12:58:07 5560.541 1800 F F 4.43 205
152100770010 263.1799 -22.9366 -92.618 2015-03-23T20:23:30 5560.851 593  F F 4.55 53
152100780010 263.1743 -22.9636 -92.628 2015-03-23T20:34:50 5560.858 2001 F F 4.57 171
152100830010 270.7986 -23.3895 -89.649 2015-03-23T23:35:02 5560.983 592  F F 4.49 60
152100840010 270.8087 -23.4127 -89.647 2015-03-23T23:46:21 5560.991 2001 F F 4.52 193
152100930010 268.4829 -23.8129 -90.586 2015-03-24T05:04:33 5561.212 2000 F F 3.65 542
152100940010 266.1420 -24.1892 -91.580 2015-03-24T05:40:05 5561.237 2000 F F 3.96 417
//
// Total vignetting corrected exposure for selected position is    8.86596e+04 s
```

C Calculating errors

All errors estimates throughout the thesis has been made conservative in order to be 'on the safe side'. If x has the error δx, the error of $F(x)$ involving a constant C:

$$F = C\,x$$

has been assigned an error estimate of:

$$\delta F = C\,\delta x$$

If $F(x)$ involves a sum or difference of $x \pm \delta x$ and $y \pm \delta y$:

$$F = x \pm y$$

F has been assigned an error of:

$$\delta F = \sqrt{(\delta x)^2 + (\delta y)^2}$$

If F involves the multiplication or division of x and y:

$$F = \frac{x}{y} \text{or} F = x\,y \tag{25}$$

F had been assigned an error of:

$$\delta F = F\left(\frac{\delta x}{x} + \frac{\delta y}{y}\right) \tag{26}$$

If F involves x raised to a power:

$$F = x^n \tag{27}$$

F has been assigned an error of:

$$\delta F = |n|\,\delta x \tag{28}$$

D XSPEC scripts

The following is the XSPEC used to calculate the persistent flux.

```
proc autorun {Burst_nr dataType} {

query yes
set fileid [open fit_BB_net.dat w]
cpd /xs

  data nu90001002002A${dataType}_sr.pha, nu90001002002B${dataType}_sr.pha
  backgrnd nu90001002002A${dataType}_bk.pha, nu90001002002B${dataType}_bk.pha

  setplot energy
  ignore **:**-3. 30.-**

  abund wilm
  xsect vern
  weight churazov

 tclout expos 1
 set pex [scan $xspec_tclout "%f"]
 set exp [format "%.2f" $pex]

  setplot reb 10 10
  setplot com r y2 0 2
  setplot com label OT NuSTAR accretion emission ${Burst_nr} 90001002002${dataType}
  setplot com label top Net persistent spectrum: absorbed PL (${exp}s)

  mo TBabs(diskbb+compTT)
 /*
  newpar 1 0.82 -1
  newpar 2 2.7
  newpar 4 0.
  newpar 5 0.4
  newpar 6 5.
  newpar 7 2.5
  fit

  flux 2. 100. err

  pl ldata ra
  cpd /ps
  pl

  log
  show

  tclout stat
  set chistat [string trim $xspec_tclout]
  tclout dof
  set d_o_f [string trim $xspec_tclout]
  puts $fileid "[lindex $chistat 0] [lindex $chistat 6] [lindex $d_o_f 0] [lindex $d_o_f 6]"
  tclout flux 1
  set fabs [string trim $xspec_tclout]
  puts $fileid "[lindex $fabs 0] [lindex $fabs 1] [lindex $fabs 2]"

  dummyrsp 0.1 100.
  flux 0.1 100.
  newpar 1 0.
  flux 0.1 100.

  tclout flux 1
  set fbol [string trim $xspec_tclout]
  puts $fileid "[lindex $fbol 0]"
  close $fileid

  exec /bin/mv pgplot.ps Pers_spe.ps
  exec /bin/mv xspec.log A+B_xspec.log

  exit
}
```

The following is an example used to calculate the characteristics of the bursts.

```
proc autorun {Burst_nr intv.dir dataType} {
query yes
cd test
set fileid [open fit_BB_net.dat w]
cpd /cps
  data nu90001002002A${dataType}_sr.pha, nu90001002002B${dataType}_sr.pha
  backgrnd ../B1_Ae/nu90001002002A${dataType}_sr.pha, ...
       ../B1_Ae/nu90001002002B${dataType}_sr.pha
  setplot energy
  ignore **:**-3. 20.-**
  abund wilm
  xsect bcmc
  weight churazov
 tclout expos 1
 set pex [scan $xspec_tclout "%f"]
 set exp [format "%.2f" $pex]
  setplot reb 20 20
  setplot com r y2 0.5 1.5
  setplot com label OT SAX J1748.9-2021 NuSTAR 90001002002 Burst ${Burst_nr}
  setplot com label top Net burst spectrum: absorbed blackbody (${exp}s)
  mo TBabs*(bbodyrad)
/*
  newpar 1 0.82 -1
  newpar 2 2.
  fit
  log
  show
  err 2 3
  flux 2. 100. err
  tclout param 2
  set par1 [string trim $xspec_tclout]
  tclout err 2
  set err1 [string trim $xspec_tclout]
  puts $fileid "[lindex $par1 0] [lindex $par1 6] [lindex $err1 0] [lindex $err1 1]"
  tclout param 3
  set par2 [string trim $xspec_tclout]
  tclout err 3
  set err2 [string trim $xspec_tclout]
  puts $fileid "[lindex $par2 0] [lindex $par2 6] [lindex $err2 0] [lindex $err2 1]"
  tclout stat
  set chistat [string trim $xspec_tclout]
  tclout dof
  set d_o_f [string trim $xspec_tclout]
  puts $fileid "[lindex $chistat 0] [lindex $chistat 6] [lindex $d_o_f 0] [lindex $d_o_f 6]"
  tclout flux 1
  set fabs [string trim $xspec_tclout]
  puts $fileid "[lindex $fabs 0] [lindex $fabs 1] [lindex $fabs 2]"
  setplot com label file kT=[lindex $par1 0]keV  BB_norm=[lindex $par2 0]
  plot ldata ra
  dummyrsp 0.1 100.
  flux 0.1 100.
  newpar 1 0.
  flux 0.1 100.
  tclout flux 1
  set fbol [string trim $xspec_tclout]
  puts $fileid "[lindex $fbol 0]"
  close $fileid
  exec /bin/mv pgplot.ps net_XrB_spe.ps
  exec /bin/mv xspec.log A+B_xspec.log
exit
}
```

DTU Space, Danmarks Tekniske Universitet
Elektrovej, building 328
2800 Kgs. Lyngby
Tlf. Tel (+45) 4525 9500
Fax Fax (+45) 4525 9575

www.space.dtu.dk